Univerzita Karlova v Praze
Matematicko-fyzikální fakulta

Diplomová práce

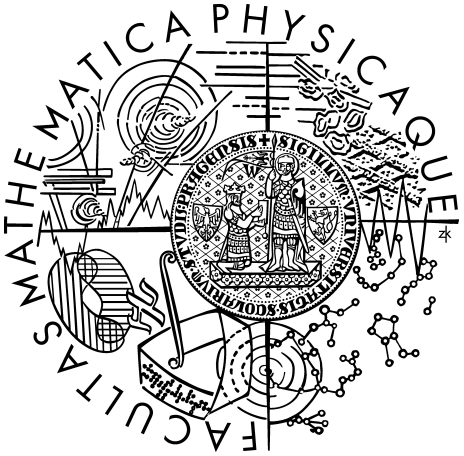

Jan Kulveit

Studium nukleace kvantových teček

Ústav teoretické fyziky MFF UK

Vedoucí diplomové práce: prof. RNDr. Pavel Demo, CSc.
Fyzikální ústav AVČR, v.v.i.

Studijní program: Fyzika-teoretická fyzika

Rád bych poděkoval prof. Pavlu Demovi za pomoc a trpělivost při vzniku této práce, a též za četné diskuse o nukleaci a fyzice obecně.

Též chci poděkovat své rodině - můj táta, František Kulveit, akademický malíř, se dokončení této práce nedožil, ale vždy mne podporoval v zájmu o fyziku, oblast krásy docela odlišnou od té, kterou se zabýval sám. Mamince Jaroslavě zvlášť děkuji za důvěru a obětavost, a za podporu a pomoc v době psaní práce děkuji Janě. Bez Vaší lásky by tato práce vzniknout nemohla.

Prohlašuji, že jsem svou diplomovou práci napsal samostatně a výhradně s použitím citovaných pramenů. Souhlasím se zapůjčováním práce.

V Praze dne 14.4.2010 Jan Kulveit

Charles University in Prague
Faculty of Mathematics and Physics

Diploma thesis

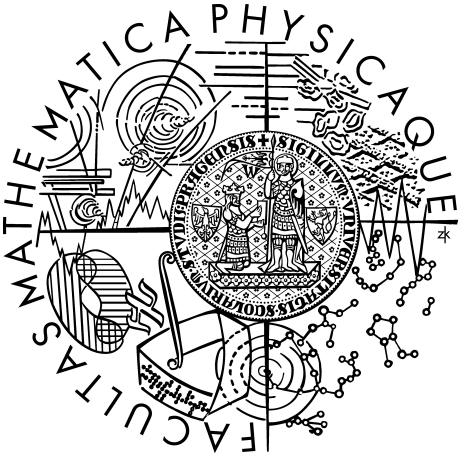

Jan Kulveit

Nucleation of quantum dots

Institute of Theoretical Physics

Supervisor: prof. RNDr. Pavel Demo, CSc.
Institute of Physics AS CR

Branch of study: Physics - Theoretical Physics

I would like to thank my supervisor prof. Pavel Demo for patience and help with this work, and also for many interesting discussions about nucletion theory and physics in general.

I also want to express my gratitude to my family - my late father František Kulveit, ac. painter, always supported my interest in physics, a field of beauty quite different from that of his own interest. I especially want to thank my mother Jaroslava for trust and self-sacrifice, and for help and support in time of writing this work I thank Jana. Without your love this work would not be possible.

I hereby declare that this thesis is my own work and all used sources are cited and acknowledged.
I agree the thesis can be made publicly available.

Prague, 14.4.2010 Jan Kulveit

Contents

Název práce: *Studium nukleace kvantových teček*
Autor: *Jan Kulveit*
Katedra (ústav): *Ústav teoretické fyziky MFF UK*
Vedoucí diplomové práce: *prof. RNDr. Pavel Demo, CSc., Fyzikální ústav AVČR, v.v.i.*
e-mail vedoucího: *demo@fzu.cz*

Abstrakt: *Kvantové tečky jsou předmětem rostoucího zájmu v mnoha vědeckých oborech. Kromě jiných metod mohou kvanotvé tečky vznikat také nukleací. V předložené práci studujeme počáteční stádium nukleace v krystalech NaCl a KCl počítačovým modelováním krystalové mříže. V systému NaCl-Pb mají nejstabilnější malé klastry rovinnou strukturu v $\{1,1,1\}_{Na}$ rovině okolní mříže a nukleuje přechodná 2D fáze. Oproti tomu v KCl-Pb jsou nejstabilnější klastry se strukturou Suzukiho fáze a nukleuje Suzukiho fáze. Vytvoření této fáze znesnadňuje další přechod ke stabilní $PbCl_2$ struktuře. Tyto výsledky počítačového modelování jsou ve shodě s experimentálně pozorovanými rozdíly v chování KCl-Pb a NaCl-Pb.*
Klíčová slova: *alkalické halogenidy, klastrování divalentních příměsí, Suzukiho fáze, nukleace*

Title: *Nucleation of quantum dots*
Author: *Jan Kulveit*
Department: *Institute of Theoretical Physics MFF UK*
Supervisor: *prof. RNDr. Pavel Demo, CSc., Institute of Physics AS CR*
Supervisor's e-mail address: *demo@fzu.cz*

Abstract: *Quantum dots are increasingly important in many fields of science. Among other methods, quantum dots can also be formed by nucleation processes. In present work we study early stage of nucleation in NaCl and KCl crystals doped with $PbCl_2$. Defect energies of small Pb clusters were calculated using numerical lattice methods. In NaCl-Pb system most stable small clusters have planar structure in $\{1,1,1\}_{Na}$ host lattice plane and intermittent planar phase nucleates. In contrast in KCl-Pb system small clusters with Suzuki phase structure are most stable and Suzuki phase nucleates. Formation of Suzuki phase hinders further transition to stable structure. These results of computer simulation are in agreemend with experimentally observed differences in KCl-Pb and NaCl-Pb systems behavior.*
Keywords: *alkali halides, divalent dopant aggregation, Suzuki phase, nucleation*

Introduction

Quantum dots[1] are subject of great interest in many fields of science, notably quantum information processing. These nanostructures can be either manufactured in so called "top-down" approach, or emerge as a product of nucleation process. As quantum dot properties are highly dependent on their size and shape, for most applications growth of structures with specified size and narrow size distribution is desirable.

In this work we study nucleation in solid-state solution of Pb dopants in two alkali halide matrices (NaCl, KCl). Particularly, one aim is to explain differences in observed behavior in the two systems by theoretical modeling. Second general objective is to gain better understandind of the system with possible application for control of nucleation process.

Thesis outline

This diploma thesis is composed of four chapters. First chapter consists of brief description of several motivations for interest in quantum dots and dopant centres. Second chapter reviews the classical nucleation theory. Different perspectives and refinements of classical theory are framed in cluster dynamics approach. Third chapter deals with nucleation of divalent impurities in alkali halide crystals and presents original results of this study concerning first stage of the process. Discussion in fourth chapter compares these results with experimental data and also previous theoretical studies. Final Conclusions summarize the results of previous chapters. Appendix gives more details and parameters of simulation method used to obtain results of Chapter 3.

[1] Terminology varies between relevant fields of research and e.g. quantum dot, nanocrystal, nucleus, and precipitate may in some situation refer to the same physical object in different descriptions. In present work consistency with terminology prevalent in mainstream literature of respective fields was usually preferred at the cost of using different terms for same object in different contexts.

Chapter 1

Motivations

Nanoworld - that is, reality at nanoscales, about 9 decimal orders of lengths far from our everyday experience - is subject of attention both scientific and popular. While the fundamental laws of quantum mechanics ruling small scales are known for almost hundred years, there is still a lot of "terra incognita". Rapid development of advanced experimental methods in recent decades allow more direct study, theory evolves, and also third general approach - computer simulations - emerged. Broad range of fields, including physics, chemistry, materials science and biology meets at nanoscale level and in a way becomes indistinguishable.

Nano-world not only offers opportunities for exploration, but also valuable resources. Perhaps, the most sought after are those which would enable sustaining of the exponential growth of computer capabilities, predicted by so-called Moore's law,[1]. Any strain of fundamental research which holds some promise of providing "basic layer" for future computers gains attention and wide range of nanoscale objects, for example carbon nanotubes, nanowires, graphene systems, macromolecules and self-assembled systems, is considered for use[2] either in new technologies or next stage of miniaturization of current technology.

1.1 Quantum computing

Probably most radical proposal for future computing architecture is quantum computing. Current and next generation[1] computer architectures are based on transfer of charge passing through transistors (basically working as switches) arranged as logical gates (e.g. AND). The logical gates operate on input consisting of bits[2], taking values 0 or 1. Physically these bits are represented by classical system - e.g., in

[1]The Moore's law states the number of transistors on typical integrated cirquit doubles approximately every two years. The law is in big part self-fullfiling prophecy, as the research and development in the field is often directed towards achieving predicted values. [1]

[2]In contemporary binary computers, generally computers with binary logic, but N-state logic is possible and some cases were explored in early digital computers.

current architecture by different levels of voltage in capacitor charged with many electrons. While mechanisms of charge-carrier transport and other details of operation of individual elements are explained by quantum theory, the computation is essentially classical. Quantum effects, such as tunneling, pose a problem for further scaling of computer elements.

Quantum computing approach utilizes quantum properties for computation, mainly the greater capacity of state space and in particular entanglement. The data are represented by qubits [63](from "quantum bit"), which correspond to state space of two-state system. Qubits can be in basis states $|0\rangle$, resp. $|1\rangle$ or any quantum superposition. In correspondence with classical computing, qubits are subjects of action of quantum logical gates - unitary operators, usually represented by matrices. Special operations are initialization of qubits to given state and measurement. Various theoretical models of quantum computation has been proposed, the canonical being a gate model - a generalization of Turing machine [50]. Among others the most perspective are cluster state computation [49], quantum adiabatic computation [26] and topological quantum computation [29].

Implications of this theoretical model - quantum computing "software" - was subject of much study in last two decades and many important results were achieved. In 1994, Shor [55] discovered famous algorithm allowing factorization of integer N in polynomial time $t \sim O((\log N)^3)$ - note $\log N$ is the length of the integer in digits or in other words the size of imput. Best classical algorithm runs in sub-exponential time $t \sim O(\exp(\log N)^{1/3}(\log\log N)^{2/3})$, hence a dramatic improvement for long imputs is possible by quantum computation. Factorization problem is not only of mathematical concern: important part of cryptography in everyday use from banking to secure email access relies on the assumption that factorization of large integers is difficult. Discovery that quantum computers would be, at least in theory, able to factorize long numbers efficiently, drew immense interest to the proposal.

Many other algorithms where quantum computing offers speedup have been discovered, notably Grover algorithm [33] allowing fast search in unsorted database. Quantum error correction codes were devised to counter errors in data representation caused by decoherence. General comparison of power of quantum and classical computation is still open problem, but known examples of algorithms seem to indicate advantage of quantum computing is highly problem-dependent. So, possibly, future quantum computers may be used for specific tasks in conjunction with future classical processors used for general computation.

In parallel to theoretical study, there is an effort to build quantum computing "hardware". More than a decade of both theoretical studies and experiments show construction of scalable universal quantum computer performing useful calculations is a problem of immense technical difficulty. Perhaps the biggest challenge is to avoid decoherence - leakage of information from the quantum system to environment. And, at the same time still allow reliable and controlable operation of universal set of quantum gates, which requires strong interactions among qubits. Above mentioned

error-correcting software measures alleviate the decoherence problem, but work only after some critical threshold of reliability of gate operation is overcome. Hence, one of the basic criteria on possible quantum computing hardware proposals is relatively long decoherence time in comparison to gate operation time. Other widely used criteria [22] state the necessity to initialize the computer rapidly to a low entropy state, and, quickly measure the state of the system - again, this ability requires strong interactions of the quantum part of the computer with "observation apparatus".

Numerous possible physical realizations of quantum information processing hardware are studied, currently at the level of experiments with individual qubits. Much larger number was proposed theoretically. Examples of actively experimentally studied systems are atom and ion traps, superconducting cirquits, "NMR" systems, optical quantum computers, and solid-state systems based either on quantum dots or impurities (discussed later). Presently it is unclear if any, of these proposals is a viable way towards universal quantum computer and it is supposed scalability of some of the proposal is severely limited. One recent trend is to combine several of the approaches. As an example - the difficulty with optical systems is that photons are hard to "store", while they are excellent for long-distance interactions. Properties of trapped ions and similar systems are often complementary - their decoherence times are long, but "addressing" individual ions in gate operations is difficult for larger numbers of ions in the trap. An architecture with micro- or nano- scaled traps with small numbers of atoms in each, connected by optical communication, may utilize advantages of both systems. Quantum dots are often crucial part of such "mixed" schemes because they interact easily with photons.

1.2 Quantum computing using quantum dots

Solid state quantum computers are attractive for several reasons. First, while in ionic traps and similar systems it is typically necessary to first "assemble" the device, in solid state the components stay "in place". Second, extensive technological knowledge about manufacturing of small structures was gathered in half century of microelectronics development. Third, the "driving circuitry" of the quantum computer is likely to be based on solid state devices, or possibly the whole quantum computer operated as a "quantum coprocessor" for specific task along a general purpose processor.

As several of the solid-state quantum computing proposals utilize quantum dots, let's first introduce this concept. Quantum dot is an object in which movement of charge carriers is confined in all directions to small space. From theoretical viewpoint it is a physical realization of three dimensional particle in a well system. The term "quantum dot" was coined for semiconductor nanocrystallites smaller than exciton's Bohr radius, but presently is used for broad range of systems fitting above given definition. In "electrostatical" dots the confinement potential is created by lithographically

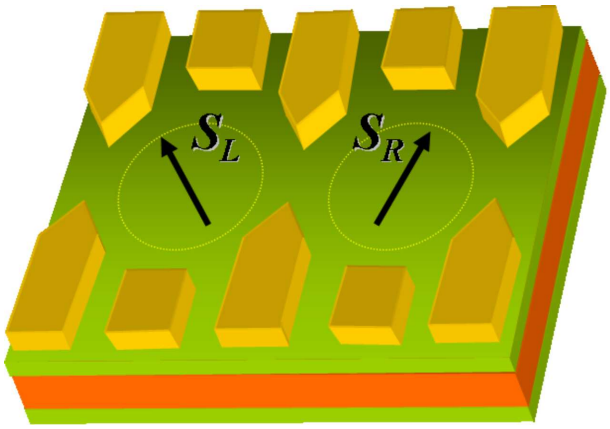

Figure 1.1: Schematic representation of coupled quantum dot system in Loss-DiVincenzo quantum computer proposal. Electrodes creating confining potential are yellow, electronic spins represented by arrows S_L and S_R. ©Dr. Vitaly Golovach, Ludwig Maximilians Universität Műnchen (reprinted with permission)

manufactured electrodes with controlled voltages, in thickness-fluctuation quantum dots by monolayer fluctuation in the width of 1-D "quantum well".

Also, from quantum computing perspective, close relatives to quantum dots are impurities in crystals. Suitable combinations of dopant (impurity) and lattice can also produce "confined" electron states. An example of system of this kind recently drawing much attention is N-V center in diamond [62], consisting of nitrogen atom substituting a carbon and negatively charged vacancy in nearest-neighbor lattice site. While the term "quantum dot" is used in following description of quantum computer proposals, the systems usually could use impurity center as well.

Having these spatially confined states, qubit can than be represented by certain two states of the system, usually charge states or spin states. As an illustrative examples, we will first describe early proposal of Loss and DiVincenzo [44] based on spin sates of single electrons confined to adjacent quantum dots with electrostatic control of gate operations. And then, recent proposal of Barrett and Kok [5] utilizing laser-driven optical transitions in single electron quantum dots.

1.2.1 Loss-DiVincenzo quantum computer

In Loss-DiVincenzo proposal [44], quantum computer is build from electrostatical quantum dots. Qubit states $|0\rangle$ resp. $|1\rangle$ are represented by spin states $|\uparrow\rangle$ resp. $|\downarrow\rangle$ of single electron confined within the dot. The dots are separated by tunneling barrier, controlled by voltage applied to central electrodes. If the barrier is sufficiently high, tunneling does not occur and individual electrons remain in initial state. Gate operation begins with lowering the barrier, so tunneling does occur, and spins are

subject to exchange interaction

$$H(t) = J(t)\hat{\mathbf{S_1}} \cdot \hat{\mathbf{S_2}}, \tag{1.1}$$

where $\hat{\mathbf{S}}$ are spin operators and $J(t)$ represents time-dependent coupling constant. By suitable time evolution of tunneling barrier, it is possible to realize so-called CNOT gate, which together with single-qubit operations form universal set capable of any computation [50]. Control of individual qubits has been demonstrated by microwave magnetic and electric fields [34]. Current experimental obstacle is decoherence of electron spin due to interaction with nuclear spins.

1.2.2 Barrett and Kok quantum computer

In this scheme qubits are also represented by electronic spin in quantum dot as before. Suitable system has low energy states $|\uparrow\rangle$ resp. $|\downarrow\rangle$, and an excited state $|e\rangle$ such that only optical transitions $|\downarrow\rangle \leftrightarrows |e\rangle$ are possible. Qubit states $|0\rangle$ resp. $|1\rangle$ are represented by $|\uparrow\rangle$ resp. $|\downarrow\rangle$.

Central part of the computing scheme is entanglement operation action on a pair of qubits. Additional facility is needed for the operation - quantum dots are embedded in open-ended resonant microcavities, tuned to the wavelength of the transition. Light escaping the cavities is mixed in beam splitter, and measured by photodetectors D_+ and D_-. Additionally single-qubit operations like initialization, flip operation X ($|\uparrow\rangle \rightarrow |\downarrow\rangle$, $|\downarrow\rangle \rightarrow |\uparrow\rangle$)) are assumed to be available. In entanglement operation,

1. the $|\downarrow\rangle$ states of both qubits are coherently pumped to $|e\rangle$
2. photodetectors wait for an event for time t_1 and further for some relaxation time
3. X operation is applied to both qubits, coherently flipping the spins
4. steps 1. and 2. are repeated (once)

Now, we can follow the system if we start from spins in non-entagled

$$(|\uparrow_1\rangle + |\downarrow_1\rangle)(|\uparrow_2\rangle + |\downarrow_2\rangle) \tag{1.2}$$

state. After the first step, the state of system under consideration changes to

$$(|\uparrow_1\rangle + |e_1\rangle)(|\uparrow_2\rangle + |e_2\rangle) \tag{1.3}$$

which we can rewrite to two qubit notation simply by multiplication of states. Hence, state of the whole system is given by

$$|\uparrow_1\uparrow_2\rangle + |\uparrow_1 e_2\rangle + |e_1 \uparrow_2\rangle + |e_1 e_2\rangle\,. \tag{1.4}$$

Now, we measure the state in step (2). If no photon is detected, we know the system is in $|\uparrow_1\uparrow_2\rangle$ state, with no entanglement. The situation is similar in detection of two photons. But if one photon is detected, the state can be either $|\uparrow_1 e_2\rangle$ or $|e_1 \uparrow_2\rangle$ and, since we have erased the path information in beam splitter, the states are indistinguishable. Hence, entanglement was formed by suitable measurement! After performing step 4., if one photon is detected in both cases, the system is fully entagled state, e.g. $(|\uparrow_1\uparrow_2\rangle + |\downarrow_1\downarrow_2\rangle)$. Theoretical maximum success rate with ideal detectors and with all emitted photos leaving the cavity to detector is 0.5, the system is indeterministic. With real detectors smaller, however, the outcome is still successful entanglement operation or unsuccessfully operation, not degradation of fidelity of quantum state.

Given entanglement operation, it is possible to construct cluster states, which were shown to be capable to simulate arbitrary logic networks. Various elements of the proposal have been demonstrated, including transfer of optical to atomic states and back [8], single-photon detection, and even photonic entanglement of atomic qubit memories at one meter distance [46] and of carbon nuclei in a diamond lattice [48].

1.3 Quantum information processing and general application

As physical realization of universal quantum computer is probably a distant goal and there are doubts if it will ever be technically feasibl [24], it is important to stress most of the elementary blocks presented here in the context of quantum computing are interesting of their own or usable in less ambitious technologies.

If we stay in the broader concept of quantum information processing, quantum cryptography is already in state of early commercial applications. Quantum cryptography solves the problem of key distribution ubiquitous in classical cryptography. Security of conventional cryptosystems relies on combination of mathematical hypotheses (such as above described assumption of difficulty of factorization of large numbers) and assumptions about computational resources of the adversary (based on aforementioned Moores law). Unexpected advances in either field can make existing cryptosystems vulnerable. In contrast, assumptions of quantum cryptosystems are only fundamental laws of quantum mechanics, and starting from these security of the system can be proved. In one conceptually simple scheme, the quantum key distribution is essentially a measurement of EPR paradox. Source emits pairs of entagled photons. Two partners wishing to securely communicate measure polarization of photons in a base randomly selected from $\{|0\rangle, |1\rangle\}$ and $\{(\frac{1}{\sqrt{2}}|0\rangle + \frac{1}{\sqrt{2}}|1\rangle), (\frac{1}{\sqrt{2}}|0\rangle - \frac{1}{\sqrt{2}}|1\rangle)\}$, and, after the measurement, exchange information about the orientations of their bases (using a reliable public channel). After some measurements, one side discloses part of the results, and the other side verifies violation of Bell inequalities. Any

attacker listening on the quantum communication channel reveals himself in deviation of measured results from predictions of quantum theory. So does any noise in the channel or error in measurement, but with known noise profile the presence of attacker can be excluded with arbitrarily low probability by disclosure of sufficient number of measurements. The secure key then consists of the undisclosed results, and can be used for further secret communication over public channel.

Existing quantum cryptography realization utilize components featured in some of the quatum computer proposals - e.g., sources of entagled photons, or single-photon detectors. On the other hand, efficiency and reach of quantum communication could be improved using quantum repeaters, relatively simple (using 100 qubits) quantum computers [35].

Another branch of quantum information devices potentially useful even if not as powerfull as universal quantum computer are quantum simulators [10], realization of Feynman's visionary 1982 idea of quantum device which would be able to simulate quantum system effectively. Universal quantum simulator equals universal quantum computer, but more limited class of simulator may be interesting. In these "limited" simulators (called also analog quantum simulators), the Hamiltonian of the simulated system is mapped onto controllable Hamiltonian of the simulator system. The concept is analogous to analog computers, which were successfully applied for simulations of classical systems, e.g., in early studies of deterministic chaos.[3] Naturally, validity of such simulations is ultimately limited by validity of theory which is used for description of the real system. Some of quantum computing proposals seem to be good candidates for quantum simulators. For example, arrays of atoms in optical lattices can be used to simulate difficult many-body problems of condensed matter physics, notably quantum phase transitions. citebuluta2009quantum.

Numerous applications of quantum dots are also available is other fields than quantum information processing. Dots are being used for example in tunable lasers, biological imaging techniques, photovoltaic, and display technology.

1.4 Manufacturing quantum dots

Generally, quantum dot manufacturing can be classified into two broad categories. In "bottom-up" approach, quantum dots are fabricated essentially by controlled nucleation (the term "self-assembly" is commonly used in this context). In "top-down" approach, dots are prepared by some macroscopic device - e.g., by lithography techniques [7].

Self-assembly of quantum dots with was successfully realized in colloids, where nucleation is controlled by adjusting temperature and concentrations of reactants.

[3] In analog computers the simulated system - described by differential equations - is mapped onto simulator system, where dynamics of the system is controllable by combination of capacitors, inductors, and resistors.

Effective nucleation control in other systems is important problem. As in most of applications, small size variation of produced quantum dots is highly desirable property, systems where nucleation and growth processes stops at some definitive small size of the growing cluster would are candidates for controlled quantum dot production.

In this study we will examine impurity nucleation in alkali halides. These systems have been experimentally studied in the Institute of Physics Academy of Sciences of the Czech Republic (FZU). The studied crystals are lightly doped with divalent impurity such as Pb and annealed at a high temperature - at the end the system is in the state of solid solution. Then, the sample is rapidly quenched, and subjected to some heat treatment. Nucleation of impurity-rich phase is them monitored mainly using optical spectroscopy.

Of particular interest in the quantum dot manufacturing context is that some earlier theoretical studies [4] concluded that in certain of these alkali halide systems, impurity aggregation process leads to exceptionally stable small cluster and ends there. Factors leading to such "limited" nucleation in solids would be interesting.

Generally, better understanding of nucleation processes is naturally important for tackling the problem of nucleation control.

Chapter 2

Nucleation theory

In Chapter 1 nucleation was presented in context of quantum dot assembly, but in broader view, it is process almost as omnipresent as phase transitions. It was studied in different transitions including condensation, cavitation, solidification, crystallization and precipitation. And in different fields of physics and technology ranging from atmospheric physics concerned with condensation of water vapor to study of damage in neutron-irradiated materials important for reactor technology applications.

In most of these situations, some general properties are the same. Discontinuous phase transitions usually proceed in three steps. First some of the small clusters of the new phase - "embryos" - appear due to stochastic fluctuations. If they reach a certain critical size, embryos become growable and stable "nuclei". This stage of the transition is called nucleation. In second stage, particles grow. Finally, in closed systems the growth is limited by supply of the untransformed, remaining phase.

Formation of nuclei is associated with an energy barrier, limiting the process, and allowing persistence of metastable phases over long periods of time. The barrier may be lowered, if the cluster forms on proper site of an existing impurity, which leads to heterogeneous nucleation. The barrier may be also lowered if the nucleus is of some intermittent phase, different in structure or composition from the stable one [53, p. 93].

In this chapter we will shortly review the classical nucleation theory and some of the modern developments and alternatives, with special attention to condensed phase.

2.1 Homogeneous nucleation without strain

We will start with the simplest case: a single component system without strain energy, such as liquid phase condensing from gas, or precipitation from liquid solution. In classical nucleation theory the capillarity approximation is frequently used - the values of the parameters used in the model are taken to be the same as in macroscopic objects

Initially, the system is in some α-phase, which is metastable with regard to phase β. In order to change to β-phase, first some small cluster of β-phase must be formed.

Energy balance for formation of a small cluster onsisiting of N particles (atoms, ions, etc.) is thermodynamically given as

$$\Delta G_N = N(\mu^\beta - \mu^\alpha) + \Delta G_{\text{interface}}, \tag{2.1}$$

where μ^β (resp. μ^α) are chemical potentials in β-phase (resp. α-phase) and $\Delta G_{\text{interface}}$ is the energy of the newly formed interface.

The first term is always negative and represents the driving force of the process. The surface term is positive and competes with the first (volume) term. For small radii, the ratio of surface to volume is large, and the surface term dominates - in effect creating a barrier for nucleation. The nature of the dependence becomes clear if we rewrite (2.1) to be

$$\Delta G_N = N(\mu^\beta - \mu^\alpha) + \eta N^{\frac{2}{3}}\sigma, \tag{2.2}$$

where η is a shape-factor surface/$N^{\frac{2}{3}}$ (constant for a given shape), and σ denotes interfacial energy per unit area (see Fig 2.1). The capillarity approximation implies the interfacial energy is assumed to be the same as for large flat interface.

For small radii, the ratio of surface to volume is large, and the surface term dominates - creating a barrier for nucleation of the height ΔG_c. Cluster of the corresponding size is known as critical nucleus N_c, with critical radius r_c, etc. While clusters smaller than N_c tend to go down the energy slope and shrink, clusters larger than N_c grow further and form stable particles of the new phase.

In this simplest case, where the interfacial energy is isotropic and the formation of the cluster doesn't cause any strains, the cluster will take spherical form. Corresponding shape factor is then

$$\eta = (36\pi)^{\frac{1}{3}} V_A^{\frac{2}{3}}, \tag{2.3}$$

where V_A is atomic volume of the cluster "building unit" (atom, ion, etc.).

2.1.1 Critical parameters - simple case

Critical parameters in this case may be easily found explicitly from the extremum condition $\partial \Delta G / \partial N = 0$:

$$N_c = \left(\frac{2\sigma\eta}{3\Delta\mu} \right)^3 \tag{2.4}$$

and

$$\Delta G_c = \frac{4\,(\sigma\eta)^3}{27\Delta\mu^2}. \tag{2.5}$$

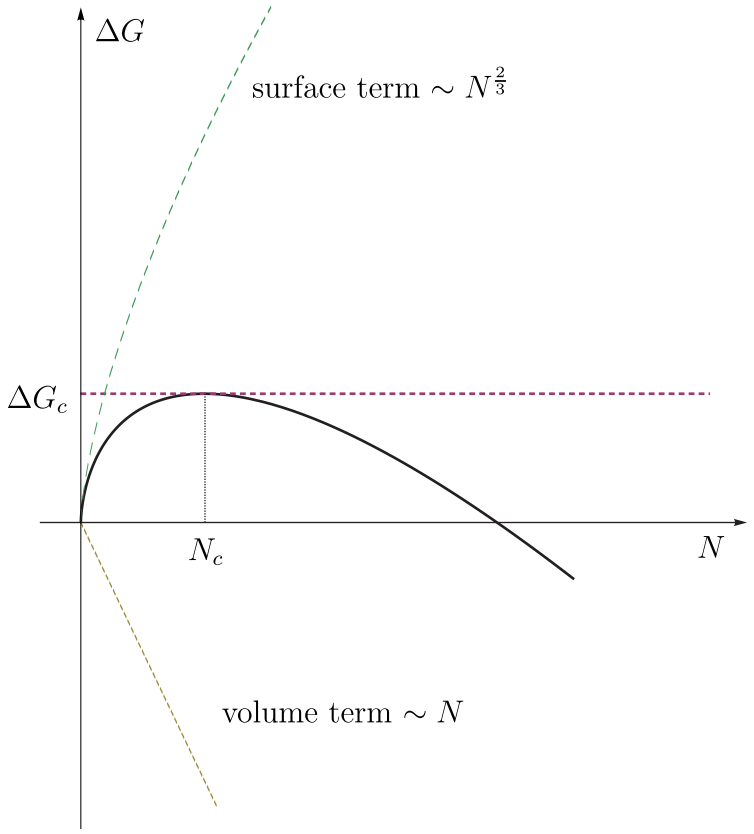

Figure 2.1: Free energy $\Delta G(N)$ as a function of cluster size N in nucleation regime

We can see that the height of the energy barrier depends on third power of surface energy σ and and on second power of $\Delta\mu$. As the change in the environment leading to nucleation is often induced by change of temperature, it is interesting to estimate the influence of temperature on the process. For example, in case of vapor condensation, we can use $\Delta\mu = kT \ln S$, where $S = p_v/p_{eq}$ is supersaturation (ratio of actual vapor pressure, p_v, to saturated vapor pressure p_{eq}). Using Clausius-Clapeyron equation

$$\Delta\mu \approx \frac{k\Delta h_{con}}{R}\left(\frac{\Delta T}{T_{con}}\right) \tag{2.6}$$

where ΔT (resp. T_{con}) is undercooling (resp. condensation) temperature, Δh_{con} is enthalpy of vaporization and R the gas constant.

Hence, the driving force of nucleation is linearly dependent on temperature - the lower the temperature, the greater the driving force.

2.2 Homogeneous nucleation with strain

To generalize our conclusions, let us consider effects of misfit of shape and size of the new nucleus within the matrix. While this effect is absent in liquid-solid nucleation, it is generally presented in solid-solid transitions. Strains act both in the nucleating particle and the surrounding matrix, thus the elastic energy of the deformation have to be accounted into the nucleation energy balance (we denote corresponding term ΔG_{el}). Furthermore, this energy also generally depends on number of building units involved within cluster, on its shape and orientation, and together with surface energy unambiguously determines properties of formed nuclei.

2.2.1 Incoherent interfaces

We start with the simplest case of acting of the strain, where the particle interface is incoherent[3, p. 597]. It means that only stress is transmitted across the interface. Strains are relaxed. As further simplification, we assume there are no pre-existing stresses in the matrix and, moreover, properties of both phases are isotropic.

Inclusion in shape of general ellipsoid of revolution was treated by Nabarro [47] within context of classical elasticity. The ellipsoid with semiaxes a,a,c (see Fig 2.2) also includes important limit cases of thin needles ($c \gg a$) and flat discs ($a \gg c$). Without any calculations, we can conclude that the strain energy, $\Delta G_{\mathrm{strain}}$, influences the nucleus shape in a different way than the surface energy: while in the limiting case of very thin disk, the strain energy would go to zero, this shape would maximize the surface energy.

Nabarro achieved general expression for strain energy per volume

$$\Delta G_{\mathrm{strain}} = 6\mu\epsilon^2 E\left(\frac{c}{a}\right), \tag{2.7}$$

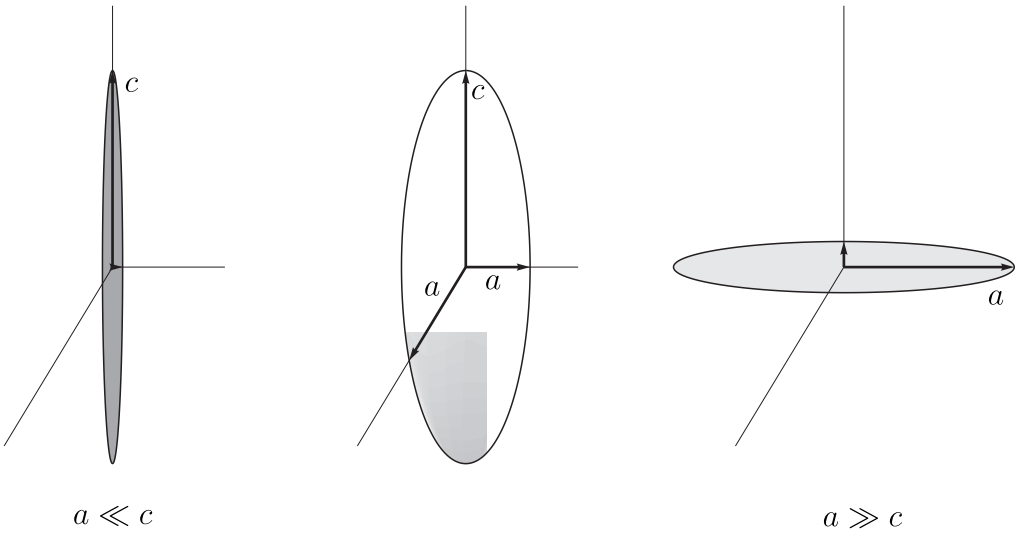

Figure 2.2: Schematic representation of various possible cluster shapes.

where shape-dependent function $E(c/a)$ is of the form, as shown in Fig 2.3 and ϵ is strain. Important conclusion is that this contribution, at least for dilute solutions (where particles are not close to each other) is volume dependent.

2.2.2 General interfaces

Case of general interfaces can be solved by following sequence of imaginary operations due to Eshelby [25].

First, the inclusion (taken as linearly elastic continuum) is cut out of the matrix. All stresses both in the inclusion and in the matrix, which now contains a cavity, are relaxed. The inclusion will assume a shape generally different from the cavity.

Second, surface tractions chosen so as to restore the inclusion to its original form are applied.

Third, the inclusion is returned back into the cavity and the interface rejoined in a way which reproduces the original interface between the cluster and the surrounding matrix. The stress is then zero in the matrix and has a known value in the inclusion.

Finally, the applied tractions are removed by applying opposite tractions of equal magnitude. The applied tractions translate to "constrained" displacements, from which strains, stresses, and eventually elastic energy can be obtained using relationships of elasticity theory.

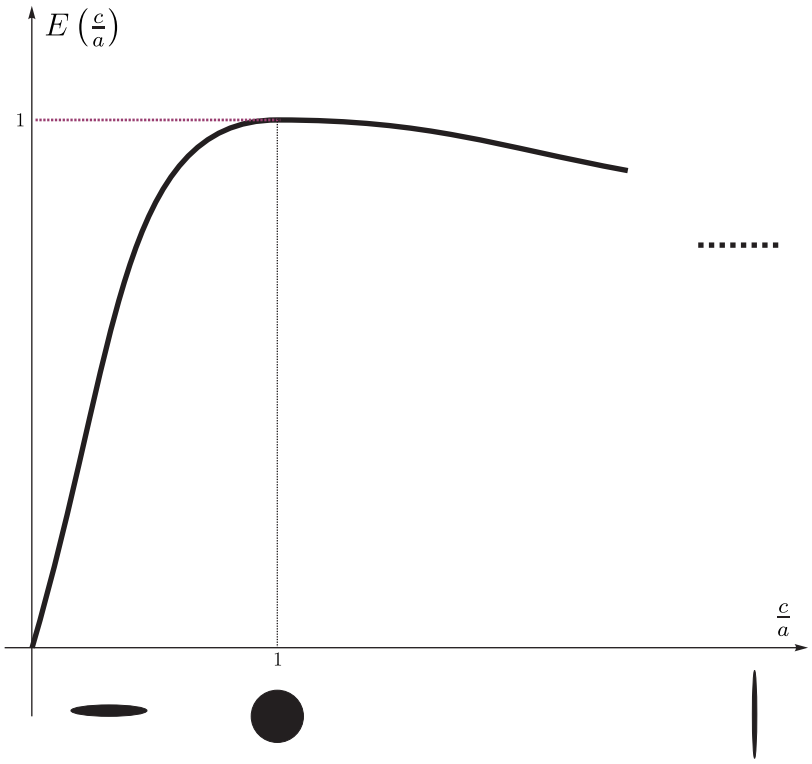

Figure 2.3: Shape dependence of strain energy. (For $c/a \to \infty$, $E = 3/4$).

2.2.3 Interface development during nucleation and growth

Above considerations lead to a picture which can be generally varied. On one side, the interfacial energy is low, if the particle keeps coherency with the matrix (if it is possible). On the other side, if there is any misfit in lattice parameters, this generates strain that eventually has to be released and the particle "breaks away". Hence, the interface looses its coherency and becomes semicoherent or incoherent.

2.2.4 Interaction with vacancies

Nucleation conditions occur frequently along with excess number of vacancies within the matrix - for example, in the case when the material is rapidly quenched from some high temperature.

The supersaturated vacancies can influence the nucleation process in two ways. They can increase the diffusion rate, and interact with incoherent (or semicoherent) interfaces acting as sources (or sinks) of vacancies. If the strain caused by the particle has positive sign (the particle would be bigger than the cavity if taken out and relaxed), a vacancy can annihilate at the interface of the particle, which in turn eliminates buildup of elastic strain energy in the lattice. Annihilation of vacancies occurs even further, until the rate at which they are removed and associated energy gain is offset by created strain energy. In the opposite case, where the strain is negative (the inclusion would be smaller when taken out of the matrix and relaxed), supersaturated vacancies impede nucleation.

We will calculate the contribution of vacancy annihilation in energy balance[3, p. 475] in the simple case of spherical inclusion. The number of vacancies removed due to formation of the cluster is proportional to the change of cluster volume:

$$N = \frac{\Delta V}{\Omega} = \frac{3\epsilon_{11}^2 V}{V_A} \tag{2.8}$$

where ΔV is change of cluster volume, Ω stands for vacancy volume. V_A stands for atomic volume, V for cluster volume and $\epsilon_{11} = \epsilon_{22} = \epsilon_{33}$ is an isotropic strain. Decrease in free energy of the system, due to relaxation of stresses, is then

$$\Delta G_v' = \frac{3\epsilon_{11}^2 V}{V_A} kT \ln(S_{vac}) = 3\epsilon_{11}^2 NkT \ln(S_{vac}) \tag{2.9}$$

with vacancy supersaturation S_{vac}.

Effect of vacancy concentration can be important and visible in the form of so called precipitate-free zones (PFZ) in metals. As vacancies are annihilated at grain boundaries, concentration of vacancies near such sinks decreases, hindering nucleation [51].

2.3 Nucleation rate

2.3.1 Classical nucleation rate

The nucleation rate is defined as a rate at which stable nuclei are formed within unit volume in unit time.

Various descriptions of the process exist. Early calculations were done by Farkas [27], steady-state calculation by Becker and Döring [6]. Here, we use cluster dynamics approach allowing derivation of both classical theory and its flavors and some of the recent models and naturally shows the links between them.

In non-nucleation regime, the new phase β is not stable, ΔG_N is always positive, no stable nuclei form and the nucleation rate is zero. The equilibrium distribution of clusters, minimizing free energy of the systems, is

$$X_N = \exp(-\frac{\Delta G_N}{\mathrm{k}T}), \tag{2.10}$$

where X_N is a fraction of clusters of size N to all clusters.

In nucleation regime, the system is out of equilibrium and clusters larger than N_c grow to stable sizes.

The growth can be described as a flux of clusters in size-space. If the coalescence rate is small (which is most often true at least at early stage of nucleation), it can be assumed that the growth is governed by single particle processes - addition or lost of one particle (the so-called step-by-step process). The cluster flux rate at one particular size can then be written as

$$J(N)(t) = \beta(N)\mathcal{F}(N) - \alpha(N+1)\mathcal{F}(N+1), \tag{2.11}$$

where $\beta(N)$ (resp. $\alpha(N)$) are transition probabilities of a particle joining (resp. leaving) a cluster of size N, and $\mathcal{F}(N)$ is a number of clusters of size N. The rate is, in general, time-dependent and the whole set of equations describing the time-dependent problem reads (using the condition of constant number of particles):

$$\frac{\partial \mathcal{F}(N)}{\partial t} = J(N-1) - J(N), \tag{2.12}$$

$$\frac{\partial \mathcal{F}(1)}{\partial t} = -2J(1) - \sum_{M>2} J(M). \tag{2.13}$$

To solve equation (2.11) we define recursive quantity Z as

$$Z(N+1) = Z(N)\frac{\alpha(N+1)}{\beta(N+1)}, Z(1) = 1 \tag{2.14}$$

summarizing information from $\beta(N)$ and $\alpha(N)$ coefficients. Z can be expressed explicitly as follows:

$$Z(N) = \prod_{M=1}^{N} \frac{\alpha(M)}{\beta(M)}, Z(1) = 1. \tag{2.15}$$

For the ratio $\alpha(N)/\beta(N)$ we have generally:

$$\alpha(N)/\beta(N) > 1 \quad \forall \quad N < N_c, \tag{2.16}$$
$$\alpha(N)/\beta(N) = 1 \quad \leftrightarrow \quad N = N_c, \tag{2.17}$$
$$\alpha(N)/\beta(N) < 1 \quad \forall \quad N > N_c, \tag{2.18}$$

$\lim_{N\to\infty} Z(N) = 0$.

Multiplying (2.11) by $Z(N)$ and summing up to $\overline{N}$, one obtains:

$$\sum_{1}^{\overline{N}} J(N)Z(N) = \sum_{1}^{\overline{N}} \beta(N)\mathcal{F}(N)Z(N) - \alpha(N+1)\mathcal{F}(N+1)\frac{\beta(N+1)}{\alpha(N+1)}Z(N+1). \tag{2.19}$$

First and second terms on the right side summation differ only in index and cancel, except at bounds of summation. Hence,

$$\sum_{1}^{\overline{N}} J(N)Z(N) = \beta(1)\mathcal{F}(1) - \beta(\overline{N}+1)\mathcal{F}(\overline{N}+1)Z(\overline{N}+1). \tag{2.20}$$

2.3.2 Nucleation rate in quasi-steady-state

For large $\overline{N}$, the second term in (2.20) can be neglected. Further, loosing generality we assume the system has reached quasi-equilibrium and the cluster flux steady-state value, $J(N)(t) = J$. (It is not a priori evident whether it is good approximation of some real systems. If it is actually good approximation or how long is the "relaxation" period before steady flux is achieved shall be discussed in Section 2.3.3.

Using above assumptions, steady nucleation rate can be expressed as:

$$J = \frac{\beta(1)\mathcal{F}(1)}{1 + \sum_{M=2}^{\overline{N}} \prod_{N=2}^{M} \frac{\alpha(N)}{\beta(N)}}. \tag{2.21}$$

To proceed further, some estimates of $\alpha(N)$ and $\beta(N)$ are necessary. One possible way is to take attachment probabilities directly from some model - which leads, for example, to kinematic nucleation theory by Katz and Weidersich [38] if attachment probabilities for gas molecules and droplets are used. But from this point we can also derive classical nucleation equation by taking the probabilities from equilibrium distribution (2.10) in true equilibrium without nucleation, or in a slightly different approach, by constructing artificial constrained equilibrium, in which cluster sizes are limited by upper boundary N_{max}, $\mathcal{F}(N) = 0 \forall N > N_{max}$.

In real equilibrium (which naturally forms a boundary condition for the nucleation), $J(N)(t) = 0$ and (2.11) becomes:

$$0 = \beta(N)\mathcal{F}(N) - \alpha(N+1)\mathcal{F}(N+1). \tag{2.22}$$

By substituting the equilibrium distribution (2.10) we get relation for transition probabilities

$$0 = N(\beta(N)e^{-\frac{\Delta G_N}{\mathrm{k}T}} - \alpha(N+1)e^{-\frac{\Delta G_{N+1}}{\mathrm{k}T}}), \tag{2.23}$$

leading to

$$\alpha(N+1) = \beta(N)e^{\frac{1}{\mathrm{k}T}(\Delta G_{N+1} - \Delta G_N)}. \tag{2.24}$$

We use this expression to solve the summation from (2.21). The inner term is

$$\prod_{N=2}^{M} \frac{\alpha(N)}{\beta(N)} = \frac{\beta(M-1)....\beta(1)}{\beta(M).\beta(M-1)\ldots\beta(2)}. \tag{2.25}$$

$$.\exp\frac{1}{\mathrm{k}T}((\Delta G_M - \Delta G_{M-1}) + (\Delta G_{M-1} - \Delta G_{M-2}). \tag{2.26}$$

$$\ldots(\Delta G_2 - \Delta G_1)) \tag{2.27}$$

$$= \frac{1}{\beta(M)}\exp\frac{1}{\mathrm{k}T}(\Delta G_M - \Delta G_1)\beta(1). \tag{2.28}$$

If we approximate summation in (2.21) by an integration, the denominator becomes:

$$\int_2^{\overline{N}} \frac{1}{\beta(M)} e^{\frac{1}{\mathrm{k}T}(\Delta G_M - \Delta G_1)}\beta(1)dM. \tag{2.29}$$

This integral depends on the given ΔG_M. We use the classical expression (2.1) based on capillarity assumption. Then, as the value of integrand is significant only near N_c, we approximate $\beta(M)$ by $\beta(N_c)$ and we extend the integration range to $(-\infty;\infty)$:

$$\int_{-\infty}^{\infty} \frac{1}{\beta(M)} e^{\frac{1}{\mathrm{k}T}(\Delta G_M - \Delta G_1)}\beta(1)dM. \tag{2.30}$$

In this approximation, we can also expand ΔG_M around N_c to second order:

$$\Delta G_M = \Delta G_{N_c} + \frac{(M-N_c)^2}{2}\left(\frac{\partial^2 \Delta G_M}{\partial M^2}\right)_{M=N_c} \tag{2.31}$$

$$= \Delta G_{N_c} - \frac{1}{3}\frac{\Delta G_c}{N_c^2}(M-N_c)^2 \tag{2.32}$$

and by solving the resulting Gaussian integral we obtain:

$$\frac{\beta(1)}{\beta(N_c)} e^{\frac{1}{kT}(\Delta G_c - \Delta G_1)}\sqrt{\frac{3\pi N_c^2 kT}{\Delta G_c}}. \tag{2.33}$$

Thus, quasi-steady-state equation for nucleation rate (2.21) in classical theory leads to

$$J = \left(\frac{\Delta G_c}{3\pi N_c^2 kT}\right)^{\frac{1}{2}} \beta_c \mathcal{F} e^{\frac{1}{kT}(-\Delta G_c + \Delta G_1)}. \tag{2.34}$$

.

The first dimensionless term is called Zeldovich factor and its magnitude is typically 10^{-1} [3, p. 466].

The ΔG_1 term in the exponent requires some explanation. It seems natural to expect the energy of "formation" of "cluster" of size 1 to be 0. But the expression for $\Delta G(N)$, (2.2) gives generally non-zero value for $N = 1$, which leads to apparently self-contradictory prediction for clusters of size 1 even in equilibrium distribution (2.10) and in all consecutive calculations. This can be understood as a result of stretching the capillarity approximation used in (2.2) clearly beyond it's limits (to a single monomer). One alternative is to use natural $\Delta G(N) = 0$. Other proposed alternative [32] is to include the term - which can be thought of as a correction to (2.2)

$$\Delta G_{NSCT} = (N-1)(\mu^\beta - \mu^\alpha) + \eta N^{\frac{2}{3}}\sigma - \eta\sigma. \tag{2.35}$$

This leads to so-called internally consistent nucleation theory.

Connection to Zeldovich-Frenkel and Turnbull-Fisher treatment

While above described expressions are quite generic, in various contexts slightly different pictures of the process are most commonly used. In condensation of vapors, the Zeldovich-Frenkel (or the Becker-Döring) picture seem to be most common versions of classical nucleation theory. The main difference of Zeldovich-Frenkel picture is use of continuum size-space from the begining, leading to immediate use of differential quantities and equations.

In context of crystallization and solid solutions, references to Turnbull-Fisher [61] picture are common, so we should make a quick connection to T-F picture.

T-F nucleation theory can be understood as a branch of above given description in the point, where estimations of $\alpha(N)$ and $\beta(N)$ are given. T-F obtain probabilities $\alpha(N)$ and $\beta(N)$ from classical reaction rate theory. An intermediate configuration (known as "activated complex") is assumed between stable clusters of size N and $(N+1)$-cluster.

The intermediate state creates additional energy barrier of height Δg above the mean of ΔG_N and ΔG_{N+1}, as shown in Fig 2.4. Transition probabilities read:

$$\beta(N) = a(N)_+ \frac{kT}{h} e^{-\frac{1}{kT}(\Delta g + \frac{1}{2}(\Delta G(N+1) - \Delta G(N))}, \tag{2.36}$$

resp.

$$\alpha(N+1) = a(N+1)_- \frac{kT}{h} e^{-\frac{1}{kT}(\Delta g - \frac{1}{2}(\Delta G(N+1) - \Delta G(N))}, \tag{2.37}$$

where $a(N)_+$ and $a(N+1)_-$ is a number of α atoms "in contact" with cluster, or number of cluster atoms in contact with α phase, and the difference between the two is considered negligible for all but smallest nuclei - $a(N)_+ \cong a(N+1)_- \cong a$. Then,

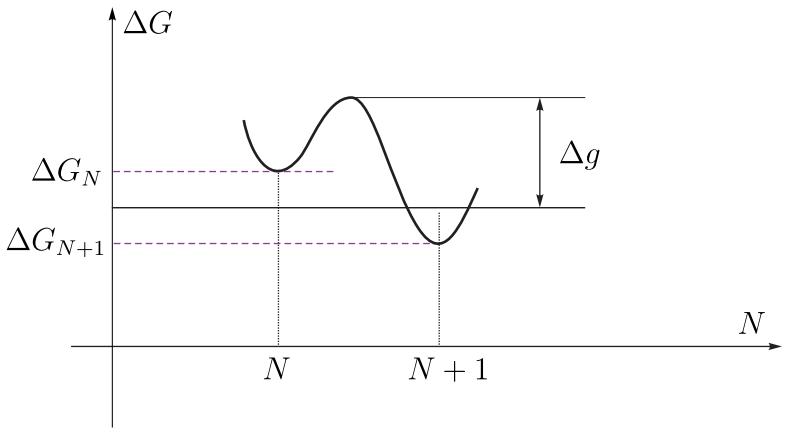

Figure 2.4: Schematic representation of energies of clusters of sizes N, resp. $N+1$ and intermediate state of higher energy.

it is possible to relate the probabilities in a way completely analogous to (2.24):

$$\alpha(N+1) = \beta(N) e^{\frac{1}{kT} - (\Delta G(N+1) - \Delta G(N))} \tag{2.38}$$

and onward proceed in the same way as from (2.24) - (2.34). As β is given more explicitly, it is possible to express also J as:

$$J = \left(\frac{\Delta G_c}{3\pi N_c^2 kT} \right)^{\frac{1}{2}} \mathcal{F} \left(\frac{kT}{h} \right) a_c \exp \frac{1}{kT} (-\Delta g - \Delta G_c + \Delta G_1), \tag{2.39}$$

where a_c is a number of surface atoms belonging to critical nucleus. The term $-\Delta g$ in the exponent may be understood to be activation energy of attachement of monomers.

2.3.3 Non-steady-state nucleation rate

To what extent the quasi-steady-state with J constant described above is a good approximation of a real physical system?

First, we can see the stationary state has to be preceded by some transition period, in which initial size distribution of clusters $\mathcal{F}(N)_0$ from non-nucleation conditions evolves to semi-steady distribution $\mathcal{F}(N)_{steady}$. This period - referred sometimes slightly ambiguously also as "incubation time" - has been subject of lot of study and both numerical and analytical solutions have been obtained.

Second, the stationarity of the state is dependent both on constant driving force $\mu^\beta - \mu^\alpha$ and constant boundary condition $\mathcal{F}(1)(t) = \mathcal{F}(1)(0)$. This can be exactly true only in open system, where number of monomers is always kept constant and approximately true in closed system, only when ratio of monomers transformed to nuclei to all monomers is negligible [41]. Otherwise, depletion of monomers lowers

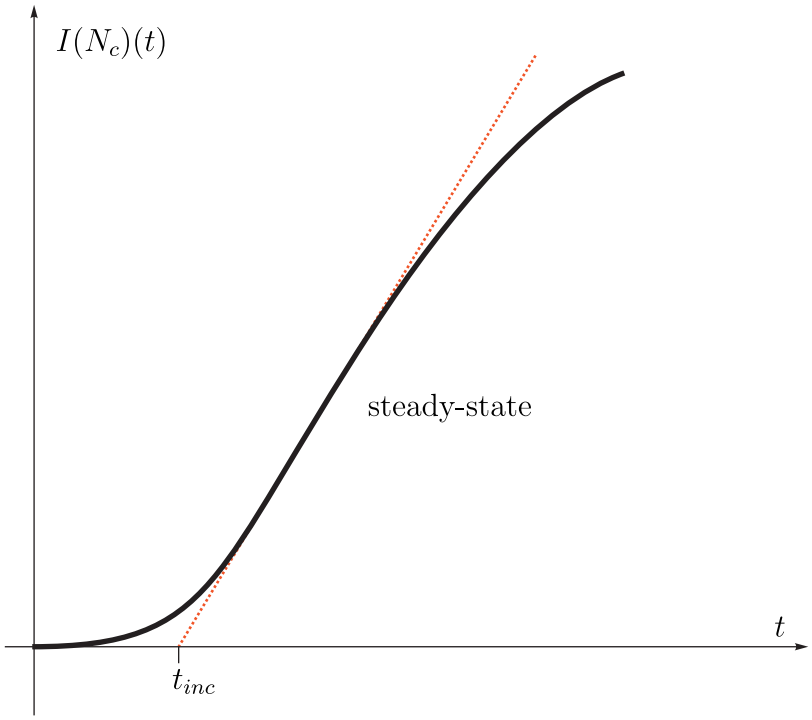

Figure 2.5: Definition of incubation time t_{inc}.

the driving force and eventually stops the nucleation. While it is shown by numerical simulations that in some situations the maximal nucleation rate achieved in the system is well bellow the "steady" rate calculated from initial supersaturation [42], this problem is less studied.

Also, other parameters of the system - such as temperature and pressure - may be, of course, varied.

Time-scale analysis of transient processes

When describing real systems often a big part of successful description is in assessment which simplifications are acceptable and which are not. A simple and useful tool for this task is time-scale analysis. So for every non-stationarity considered we will try to obtain some time scaling constant characterizing the process.

Transient nucleation rate

The time dependence of number of nuclei in a system (where steady-state was achieved) is shown in Fig 2.5. Convenient parameters to describe the evolution are J_{ss} and incubation time t_{inc}, defined as time lag to crossing point of the tangens of the growth curve in steady-state with time axis (see Fig 2.5).

Analytical treatments of the transient period have most often been based on Z-F continuum approximation. We substitute equilibrium rates (2.24) to (2.11) dividing by equilibrium distribution (2.10):

$$J = \beta(N)\mathcal{F}_{eq}(N)\left(\frac{\mathcal{F}(N)(t)}{\mathcal{F}_{eq}(N)} - \frac{\mathcal{F}(N+1)(t)}{\mathcal{F}_{eq}(N+1)}\right). \tag{2.40}$$

We express the flux in differential terms together with (2.12):

$$J = -\beta(N)\mathcal{F}_{eq}(N)\frac{\partial}{\partial N}\left[\frac{\mathcal{F}(N)(t)}{\mathrm{N}_{eq}(N)}\right] \tag{2.41}$$

$$\frac{\partial \mathcal{F}(n)}{\partial t} = -\frac{\partial J(n)}{\partial n}. \tag{2.42}$$

$$\tag{2.43}$$

Using classical expression for nucleation barrier (2.2), suitable boundary conditions

$$\mathcal{F}(N)(t=0+) = \mathcal{F}_{eq}(1)\Theta(N-1), \tag{2.44}$$

$$\left[\frac{\mathcal{F}(N)(t)}{\mathcal{F}_{eq}(N)}\right]_{N\to 1} = 1, \tag{2.45}$$

$$\left[\frac{\mathcal{F}(N)(t)}{\mathcal{F}_{eq}(N)}\right]_{N\to +\infty} = 0, \tag{2.46}$$

$$\tag{2.47}$$

where Θ is the Heavyside function. Approximate solution in good agreement with exact numerical solutions was found by Demo and Kožíšek [20].

$$\mathcal{F}(N)(t) = \frac{1}{2}\mathcal{F}_{eq}(N)\mathrm{ercf}\left(3ZN_c\sqrt{\pi}\frac{\left[(N/N_c)^{\frac{1}{3}} - 1\right] + (1 - N_c^{-\frac{1}{3}})e^{-t/\tau}}{\sqrt{1-e^{-2t/\tau}}}\right) \tag{2.48}$$

and corresponding cluster flux at critical size

$$J(N_c)(t) = J_s\frac{1}{\sqrt{1-e^{-2t/\tau}}}\exp\left(-3ZN_c\sqrt{\pi}\frac{(1-N_c^{-\frac{1}{3}})e^{-t/\tau}}{\sqrt{1-e^{-2t/\tau}}}\right) \tag{2.49}$$

where J_s is the steady-state flux (2.34). Z is the Zeldovich factor and $\tau = 7/(10\pi Z^2\beta(1))$. Often used are also older approximate solutions by Trinkaus and Yoo [60] and Kashchiev [37].

We can observe (2.49) behaves as expected - for long times $J(N_c)(t\to\infty) = J_s$ and for very short times $J(N_c)$ is exponentially small. Unfortunately, relation of time scale constant τ to incubation time t_{inc} defined as above is not easy. We need to

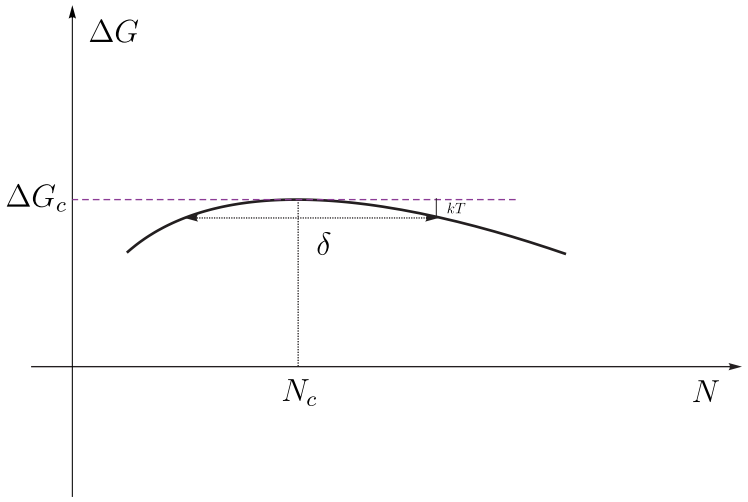

Figure 2.6: Variation of free energy in the critical region of sizes close to N_c

calculate integrated cluster flux at N_c (the cluster flux in transient regime depends on cluster size) to be

$$I(N_c)(t) = \int_0^t J(N_c)(t)dt, \tag{2.50}$$

which is an important measurable quantity on its own. Then t_{inc} can be determined from linear part of this dependence.

While above described solutions are much more accurate, simple physical picture and simpler approximations can lead to qualitative understanding of the process. Close to critical size N_C, the ΔG_N becomes more and more flat. Hence, transition probabilities are almost the same, and relation (2.11) can be approximated by

$$J(N)(t) = \beta(N)(\mathcal{F}(N) - \mathcal{F}(N+1)) \tag{2.51}$$

In continuum approximation,

$$J(N)(t) = -\beta(N)\frac{\mathcal{F}(N)}{N+1}. \tag{2.52}$$

This is equivalent to a simple diffusion equation in presence of only concentration gradient, so the movement of the cluster in size-space in the vicinity of N_C exhibits character of a random walk. Further, the movement may be understood to be a diffusion in a presence of a certain potential. So, the time lag consists of time necessary to reach the critical region in the vicinity of N_C plus the time to random walk the distance where the potential is flat. Natural boundary of the critical region is such that the potential deviates from flatness less than kT - as shown in Fig 2.6.

The distance of random walk is denoted δ. As expected, absolute value displacement of random walk after n jumps is $\sim \sqrt{n}$, the necessary time is then

$\tau \approx \delta^2/2\beta(N_c)$. Using expansion of ΔG_N from (2.31) we easily get

$$\delta^2 = \frac{kTN_c^2}{3\Delta G_c}. \tag{2.53}$$

Hence,

$$\tau \approx \frac{kTN_c^2}{6\Delta G_c \beta(N_c)} = \frac{1}{18\pi Z^2 \beta(N_c)}, \tag{2.54}$$

which has the same form as time scale from (2.49) and as several scales used in approximate solutions reviewed by Kelton [39]. As various authors use different definitions of transition rates, direct comparison is somewhat difficult.

2.3.4 Nucleation and growth

In closed systems, rapid nucleation progress changes the untransformed part of the system, which often provides negative feedback for the process.

If the process is driven by supersaturation and, moreover, the mobility of monomers is low, composition in vicinity of nuclei changes, generating concentration gradients. Consequently, the growth becomes limited by drift rate.

If the process is driven by supersaturation and the mobility of monomers is sufficiently high (it is true in the case of condensation), the concentration gradients quickly relax and supersaturation is lowered in whole system.

In both cases, the greater the initial supersaturation, the more pronounced the changes are.

Growth and nucleation processes compete: smaller particles may become unstable under decreasing supersaturation, bigger particles may grow at their expense ("coarsening").

Transition from nucleation to growth

In the cluster dynamics approach we follow, the growth region corresponds to condition $N > N_c$ where movement in cluster space is driven by drift. We can average over random fluctuations and rewrite the master equation (2.11) as

$$J(N)(t) = \gamma(N)\mathcal{F}(N), \tag{2.55}$$

where $\gamma = \beta(N) - \alpha(N+1)$ is growth rate. Now, if we describe instead of flux of cluster at specific N an average growth of a single large cluster of size $n(t)$, the descriptions are related simply by

$$\frac{dn}{dt} = \gamma(N). \tag{2.56}$$

Some classical models (such as T-F (2.36)) describe certain systems well up to arbitrary size - in large cluster limit the T-F model predicts [19]

$$\gamma(N \to \infty) = a(N)\frac{kT}{h}e^{-\frac{1}{kT}\Delta g}\sinh\left(\Delta\mu/2kT\right). \tag{2.57}$$

. Translated to single-cluster, the T-F model describes surface limited growth. As $a(N) \sim N^{2/3}$,

$$\frac{dn}{dt} \sim n^{2/3}, \tag{2.58}$$

and, asymptotically,

$$n \sim t^3. \tag{2.59}$$

Be similar reasoning we can account for any "monomer supply" limiting effect in cluster dynamics - given the model of growth of big cluster, we have also $\gamma(N)$ (for large N).

Diffusion limited growth

If the process is driven by supersaturation and the mobility of monomers is sufficiently low, composition in the vicinity of nuclei changes, generating concentration gradients. Then growth becomes limited by drift rate.

This is often the case in solid-solid transformations, as atomic jump processes are relatively slow.

Consider the simple case of spherical nucleus of β-phase of composition $c_{\beta\alpha}$ growing in α-phase with composition c_0 in untransformed region and $c_{\alpha\beta}$ at the boundary of the nucleus. We take advantage of the spherical symmetry of the problem and write diffusion equation in spherical coordinates as:

$$\frac{\partial c_{alpha}}{\partial t} = D_\alpha \nabla^2 c = D_\alpha \frac{1}{r^2}\left[\frac{\partial}{\partial r}\left(r^2\frac{\partial c_\alpha}{\partial r}\right)\right]. \tag{2.60}$$

Fick's law (flux of β particles), again written in spherical coordinates, reads:

$$J(t) = -D_\alpha \frac{\partial c_\alpha}{\partial r}, \tag{2.61}$$

where D_α is the diffusion coefficient. Flux at the interface determines the growth of the particle. Natural condition describing this fact (the so-called Stefan condition) is

$$\frac{dR}{dt}(c_{\beta\alpha} - c_{\alpha\beta}) = D_\alpha\left[\frac{\partial c_\alpha}{\partial r}\right]_{int}, \tag{2.62}$$

where we have introduced the radius of the particle to be R. Boundary conditions of constant concentration far away from the cluster and of the cluster are can be written as

$$c_\alpha(R,t) = c_{\alpha\beta}, \tag{2.63}$$

resp.

$$c_\alpha(R \to \infty, t) = c_0. \tag{2.64}$$

Exact solution of this system of equations is possible, albeit technical, but approximate solution can be derived briefly.

We can easily find "stationary" solution to diffusion equation (2.60) (under approximation $dR/dt \simeq 0$):

$$c(r) = c_0 - \left(\frac{R}{r}\right)(c_0 - c_{\alpha\beta}) \tag{2.65}$$

Hence,

$$\left[\frac{\partial c_\alpha}{\partial r}\right]_{r=R} = -\left(\frac{R}{r^2}\right)(c_0 - c_{\alpha\beta}) = \frac{c_{\alpha\beta} - c_0}{R} \tag{2.66}$$

and substituting to (2.62) we easily get

$$R^2(t) = 2tD_\alpha \frac{(c_{\alpha\beta} - c_0)}{(c_{\beta\alpha} - c_{\alpha\beta})}. \tag{2.67}$$

Rewritten in terms of n, the growth regime is of $n \sim t^{\frac{3}{2}}$ form.

Time-scale analysis

Time-scale analysis of the previous nucleation-growth transition can by carried out by concept of "transformation time" intoduced by Demetriou [19]. The total portion of nucleated phase β can be expressed as

$$X(t) = \int_0^t \overline{n}(t - t')(N_g)J(N_g)(t')dt', \tag{2.68}$$

where N_g is a size at which cluster evolution is dominated by growth - an approximation by N_c is sufficient enough. The convolution $\overline{n}(t - t')(N_g)$ gives the size of a cluster (in time t) which has size N_g in time t'.

For the purpose of time-scale analysis, it is sufficient to use "steady state" nucleated portion:

$$X_s(t) = J_s \int_0^t \overline{n}(t - t')(N_g)dt' \tag{2.69}$$

and for a growth function of a general form $C.t^p$ with arbitrary constant C this can be further simplified to form

$$X_s(t) = J_s \frac{1}{p+1} C t^{p+1}. \tag{2.70}$$

Natural time scale is given by $X_s(t) = 1$, so that

$$\tau_{tr} = \left(J_s \frac{1}{p+1} C t^{p+1}\right)^{-1}. \tag{2.71}$$

Chapter 3

Nucleation of divalent-ion impurities in alkali halides

Nucleation of divalent-ion impurities in alkali halides has been experimentally studied in the Institute of Physics Academy of Sciences of the Czech Republic (FZU), mainly using optical spectroscopy.

The studied systems are crystals of alkali halide, mostly NaCl and KCl, doped with divalent impurity such as Pb, in low concentration (of order 10^{-3}/ mol). The experimental setting is generally this: first the sample is annealed at a high temperature, which leads to dissolution of any existing precipitates - at the end the system is in the state of solid solution. Second, the sample is rapidly quenched - the system becomes supersaturated solution. Then, the system is subjected to some heat treatment - aged at a temperature in range of 100 °C to 200 °C.

During the process, optical properties of the crystal are monitored in the transparency window in UV region from 200 to 400 nm. The measurement is non-destructive, allowing repeated measuremnts of single sample.

In this chapter we try to develop better understanding of the system. We will focus our attention on comparison of NaCl and KCl crystals doped with $PbCl_2$, as these cases were most studied in FZU. There is marked difference in their nucleation behavior clearly observable in experiment, and succesful description of nucleation must be able to explain the differences between the two systems.

3.1 Introduction and state of the art

Alkali halides are belong to most studied ionic solids in general. Their relatively simple structure allows modelling of some of their properties very simply - for example a model of ensemble of hard charged spheres interacting electrostatically predicts correctly many basic features of the crystal including trends of lattice energy, and nearest-neighbor distances [40].

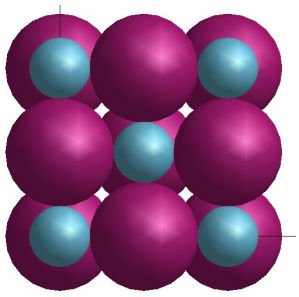

Figure 3.1: NaCl crystal in 100 plane, Cl ions violet

Apart from often being used as a textbook example, the exceptional simplicity of ideal alkali halide ideal crystals also led them to often be a system of choice for theoretical study of more complicated phenomena observed in real crystals. Important class of these are crystal defects, and of interest to this work, divalent impurities.

Doping of the crystal is often observable as a colorization of the crystal itself, hence class of color centres is associated with such defects. Even the more specific class of divalent impurities was studied for a long time. Burstein et al. [11] observed additional bands which vary with growth and thermal history of a crystal, and suggested a nucleation process as a reason. Reviews of the field by Seitz [54] note observed dependence of absorption spectra on previous heat treatment of the samples and mention aggregation of impurities as possible cause. Seitz also describes several experimental methods different from optical measurements used to study the system, including measurements relating divalent-anion concentration and conductivity, [1] and density measurements. From the experiments, estimation of association energies of impurity-vacancy complex were made, and the same quantity was also estimated theoretically.

The systems were also studied by X-ray diffraction. Of those studies the most important were by Suzuki [45][58] in 1954 and 1955 on NaCl-$CaCl_2$ mixed crystals. In this work, Suzuki observed larger impurity precipitates, and proposed model for their structure explaining observed X-ray diffractions, consisting of formation of thin plate-zones in {111} and 310 planes, consisting of thinner "platelets" - impurity and vacancy aggregation zones coherent with surrounding lattice yet resembling structure of $CaCl_2$. This conclusion was further confirmed by observation that subsequently forming crystals of $CaCl_2$ structure incoherent with the NaCl matrix were also in corresponding orientation relationship with mother lattice (e.g. $111_M/100_{precip}$). Both the observed patterns and their interpretation is analogous to patterns observed in age hardened alloys (so-called Guinier-Preston zones) [3, p. 557].

[1] Introduction of divalent ion creates a vacancy to maintain neutrality of the crystal. In lower temperatures number of such vacancies dominates over thermally induced vacancies, hence in concentrations from 10^{-5} conductivity is determined mostl by the impurity concentration

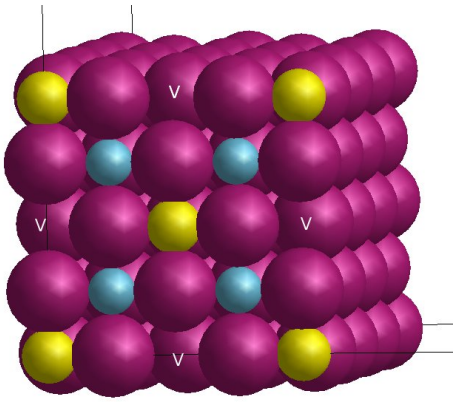

Figure 3.2: Suzuki phase unit cell in NaCl crystal in 100 plane, Cl ions violet, Pb ions yellow. Vacancies indicated by letter V.

In his later pioneering work [59], Suzuki studied NaCl-$CdCl_2$ system and explained observed patterns by emergence of new metastable phase (now called Suzuki phase), with primitive unit cell edge twice the size of NaCl primitive cell edge, and of $CdCl_2$.6NaCl stechiometry. (Suzuki phase unit cell in KCl is shown in Fig 3.2). The Suzuki phase maintains consistency with NaCl lattice.

Aggregation of divalent-ion vacancy pairs was a topic considerable interest. Careful dielectric, UV absorption and emission studies were made particularly by Dryden [15][16][23] in NaCl-$CaCl_2$, NaCl-$MnCl_2$, KCl-Sr_2 and KCl-$CaCl_2$ systems. Similar measurements have been made by Capelletti and Benedetti [12] in NaCl-$CdCl_2$.

Models of initial steps of nucleation have been developed. Dryden suggested [16] third-order reaction of dipoles to from trimmer of a hexagonal structure (corresponding to $T3$ in Fig 3.5), and, subsequently, by addition of two dipoles a time to form a pentamer, heptamer, etc.

In 1980, theoretical studies were done by Corish et al. [17] and Bannon et al. [4]. To author's best knowledge, the most comprehensive studies until now are computations of defect-cluster energies in NaCl:Mg_2, KCl:Mg_2 and KBr:Mg_2 by Corish et al. [17] and of Mn, Cd and Pb incorporated in NaCl, KCl and KBr structures by Bannon et. al. [4]. Results of these studies will be further referenced below.

So a short summary of present state of theory of $PbCl_2$ cluster nucleation in NaCl and KCl could be this: At least, since Burstein it was speculated substantial part of the driving force for nucleation is the lattice strain caused by different ionic radii of the impurity and the anion. Dryden [16] proposed model where in first stage three dipoles form a hexagonal trimmer, and in second stage clusters of 5,7,9,... etc. dipoles are built from the trimer. The model can be described formally by reaction equations

$$3X_1 \Leftrightarrow^{k(1)}_{l(2)} X_3 \tag{3.1}$$

and

$$X_{2N+1} + 2X_1 \Leftrightarrow_{l(2N+2)}^{k(2N-1)} X_{2N+2}, \tag{3.2}$$

where X_N are, respective, cluster concentrations and k rate constans. Dryden also modelled cluster size distribution in time, with rate constants k chosen to fit the experimental data. Differing model by Strutt and Lilley [57] supposed precipitation of Suzuki phase. Crawford [18] improved model of Dryden assuming intermediate dimer formation, which was supposed to be more plausible than reaction of third order (direct formation of the trimer from three dipoles) originally proposed by Dryden.

In calculations of Bannon et al. [4], most stable small cluster for both systems is the hexagonal trimer plane described by Dryden, but for KCl the stabilization energy of this trimer was smaller than stabilization energy of bulk Suzuki phase. Bannon concluded that aggregation of *nn* dipole leads to this exceptionally stable hexagonal trimer, and for some systems the process ends there. For other systems, where the stabilization energy of Suzuki phase would be higher, the dipoles are likely "converted" in the dimer stage to *nnn* form more suitable for formation of Suzuki phase. Aggregation of such dipoles than leads to aggregation of Suzuki phase and, eventually, growing Suzuki phase causes redissolving of trimers. This aggregation path remained somewhat unexplained by results of the calculations.

Later studies confirmed nucleation of Suzuki phase aggregates in some systems [28], or calculated energy of Suzuki phases by high quality ab initio computations [14], but these results were often limited to a single alkali halide - impurity system. While the studies are of high precision, they are also mostly of limited use in explaining the nucleation behavior. Surprisingly, while Suzuki phase remained a topic of sustained attention since its proposal, the model of "platelets" occurring in NaCl-$CaCl_2$ also from Suzuki was not considered in most of later studies. Recently Polak et.al [36] suggested difference in behavior of NaCl and KCl in terms of intermediate formation of some complex lead halide (e.g. $KPbCl_3$) which does not exist in case of Na-Pb-Cl system, and modeled aggregation of $PbCl_2$ in NaCl by classical nucleation theory.

3.2 General properties of system

NaCl - the rock salt - is one of the most studied alkali halides. It forms a ionic crystal with fcc lattice.

$PbCl_2$ occurs in nature as a mineral called cotunnite. Under normal conditions it forms rhomboedric lattice with Pbma symmetry. The structure is difficult to describe in simple terms, but can thought of as deformed hexagonal packing of chlorine ions with smaller Pb^{2+} stacked in between in every layer. (View of 001 plane is in Fig. 3.10).

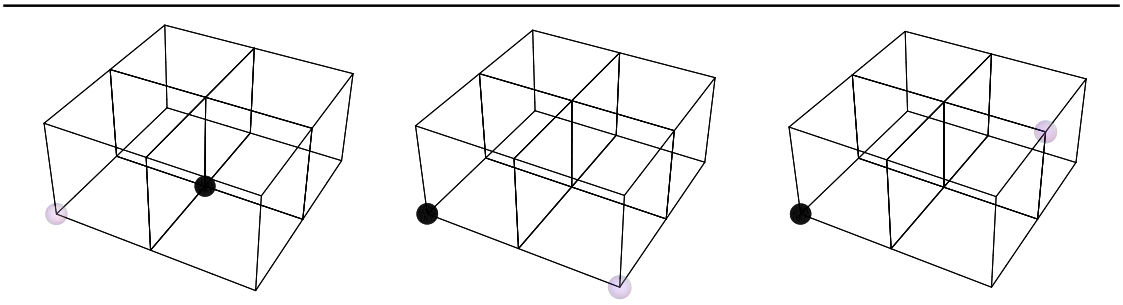

Figure 3.3: Impurity-vacancy complexes in nearest neighbor (nn), next-nearest neighbor (nnn) and second-next-nearest neighbor ($n2n$) configurations. Impurity is represented by dark sphere, vacancy by light sphere, other points belong to NaCl lattice.

3.3 Cluster energies in NaCl-$PbCl_2$ and KCl-$PbCl_2$ systems

We shall start with consideration of the behavior of "isolated" Pb centres in the crystal. In temperature region where the samples are aging, Pb forms Pb^+ - cation vacancy complexes (dipoles). From the standpoint of nucleation theory, we view these dipoles as "monomers". First step in understanding the precipitation behavior is calculation of vacancy and isolated impurity energies and dipole energies for various possible configurations. Second, we will calculate energies of some larger complexes.

3.3.1 Method of calculations

All the defect energies mentioned here were calculated by method described in detail in Appendix A. Generally, the defects were embedded in cluster containing 1229 ions. Classical lattice relaxation based on Ewald summation and pair interionic potentials was used for optimization of energy of the structure. Computations were done using program GULP [31] and some auxiliary original code developed by author. Empirical interionic potentials (IOPs) by Catlow [13] were used for description of mother phase interactions, and an original potential for Pb-Cl interaction was created by fitting empirical data of $PbCl_2$ structure. IOP parameters are listed Appendix A.

3.3.2 Dipoles

Several dipole configurations are illustrated in Fig 3.3 and energies in Table 3.1.

The more interesting quantities are dipole binding energies,

$$\Delta U(nn) = U(nn) - U(I) - U(V) \tag{3.3}$$

Dipole energy	$U(c)$		ΔU		ΔS
System	NaCl:Pb	KCl:Pb	NaCl:Pb	KCl:Pb	
impurity	-10.31	-11.49			
vacancy	4.92	5.06			
nn	-6.03	-7.15	-0.64	-0.73	-2.14×10^{-4}
nnn	-5.94	-7.09	-0.55	-0.67	-1.54×10^{-4}
$2nn$	-5.84	-6.85	-0.45	-0.42	-2.73×10^{-4}
Experiment			ΔU		
			-0.63		
			-0.780		

Table 3.1: Dipole energies in eV, configurational entropy in ev.K^{-1}. ΔU is energy of association. ΔS is configurational entropy of cluster. Experimental values are determined from diffusion measurements for two different NaCl crystal by Krause and Fredericks. [43]

$$\Delta U(nnn) = U(nnn) - U(I) - U(V) \tag{3.4}$$

and

$$\Delta U(n2n) = U(n2n) - U(I) - U(V) \tag{3.5}$$

where I denotes impurity, V vacancy and nn etc. dipole configurations. A larger negative value of the difference means more strongly bound and more stable dipole. Table 3.1 shows that in both system the nearest neighbour (nn) configuration is more stable (although in KCl the difference is smaller).

Also notable is the contribution of configurational entropy of various clusters. While above given calculation list internal energies of formation, the quantity which governs what objects will be present is free energy difference of cluster formation (discussed in Chapter 2), defined as T $\Delta G = \Delta U - T.S$ At temperature 300 K the $T.S$ term between nnn and $2nn$ clusters is 0.05 eV, which is comparable to the differences in internal energies of the configurations. Also, differences in energies are only of order away from $kT = 0.03$eV at 300 K. This indicates different dipoles will be present in substantial concetration. Important quantity for the description of the process is diffusion coefficient of the dipoles.

3.3.3 Dimers to tetramers

While in the case of dipoles, examination of all possible configurations up to some distance was done, for dimers, trimers, and higher aggregates the situation is more complex. An exhaustive search in configurational space would be computationally

Cluster energy	$U(c)$		ΔU	
System	NaCl:Pb	KCl:Pb	NaCl:Pb	KCl:Pb
$D1$	-12.20	-14.53	-0.14	-0.23
$D2$	-12.24	-14.31	-0.18	-0.01
$D3$	-12.28	-14.52	-0.22	-0.21
$D4$	*-12.39	-14.57	-0.34	-0.26
$D5$	-12.25	-14.50	-0.28	-0.25
$D6$	-12.17	*-14.76	-0.29	-0.57
$D7$	-10.60	-13.14	1.37	1.11
$D8$	-12.26	-14.40	-0.20	-0.09
$D9$	-12.19	-14.55	-0.13	-0.24

Table 3.2: Cluster energies of dimers (in eV). ΔU are energy differences between a cluster and its constituent dipoles (nn or nnn). Most stable configurations are marked *.

very expensive, so we decided to "follow" the growth and examine only clusters which can be obtained from $(N-1)$-particle clusters by addition of single dipole to most stable conflagrations(s), with some arbitrary manual pruning of the configuration space and some additions. All configurations present in previous studies of Corish et al. and Bannon et.al. have been also included.

Some interesting dimer configurations (labelled DN, $N = 1, 2, \ldots$) are illustrated in Fig 3.4 and their energies are given in Table 3.2. Selected trimer and tetramer configurations in Fig 3.5 and respective energies in Table 3.3. (Labeled TN, resp. QN, $N = 1, 2, \ldots$.)

Again, for most purposes energy differences between various configurations are of high interest and not isolated values. Calculated are internal energy differences of formation of the cluster CN formed from cluster BM and $D2$

$$\Delta U(CN) = U(CN) - U(BM) - U(nn) \tag{3.6}$$

The gigher negative value, the greater stabilization; positive value would indicate a presence of nucleation barrier.

KCl

In case of KCl, the most stable dimer is quadrupole $D2$, most stable trimer is $T2$, and generally, the initial steps of aggregation seem straightforward. The emerging structure is a face of Suzuki phase cell. Calculated energy differences between simple planar growth $Q7$ and three dimensional configuration identical to quarter to Suzuki phase unit cell $Q8$ are negligible.

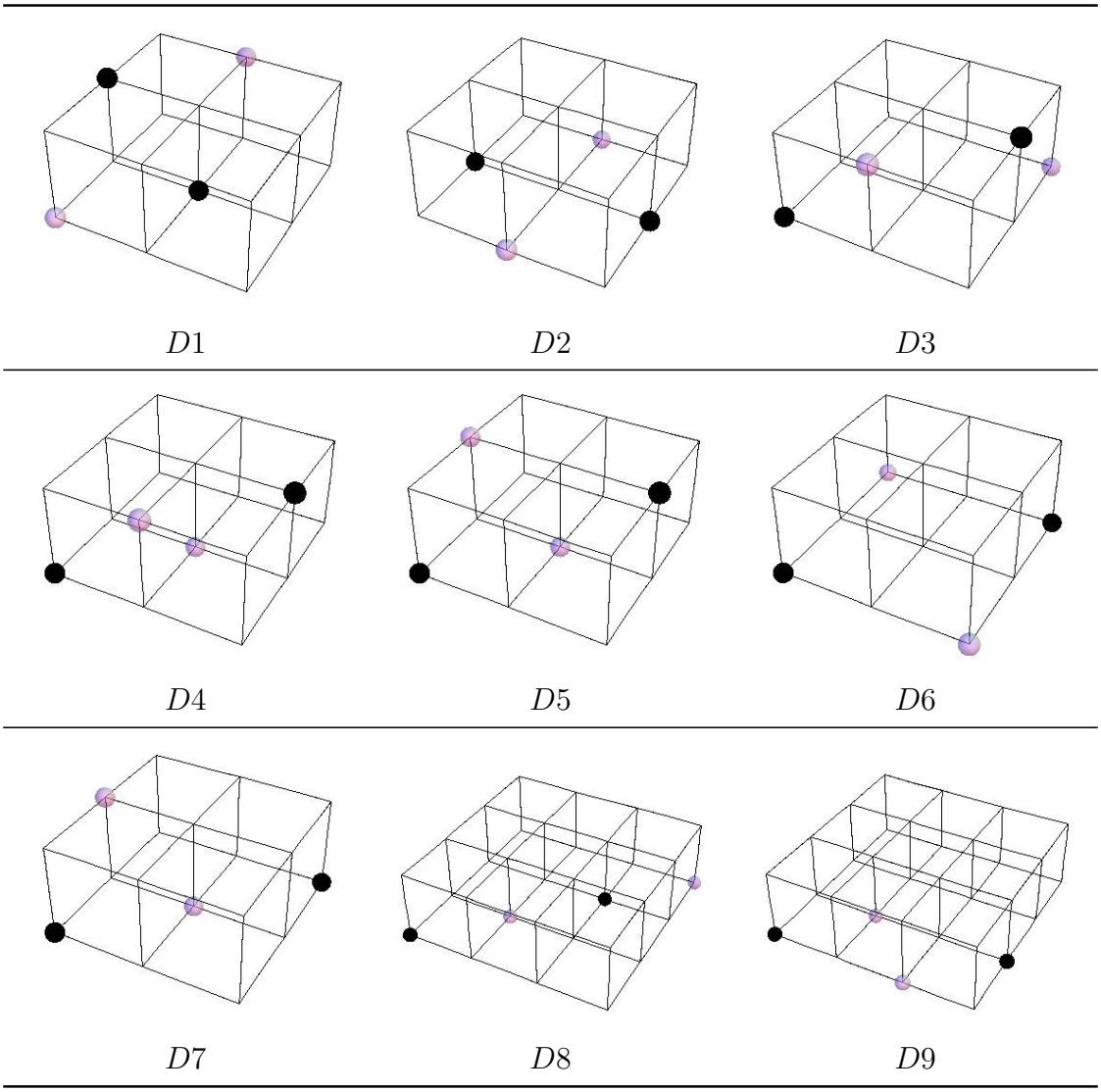

Figure 3.4: Various configurations of dimers (clusters of two dipoles). Impurities are represented by dark spheres, vacancies by light spheres, other points belong to NaCl lattice.

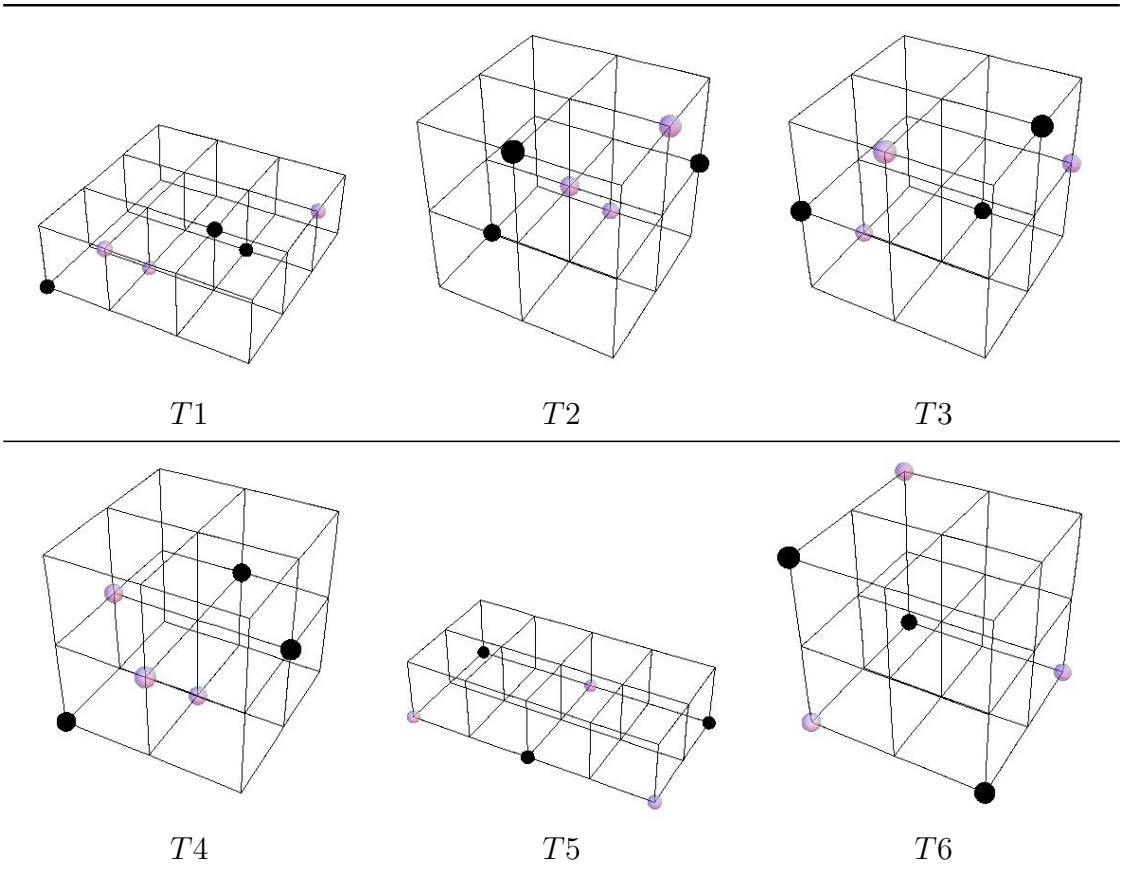

Figure 3.5: Selected configurations of trimers

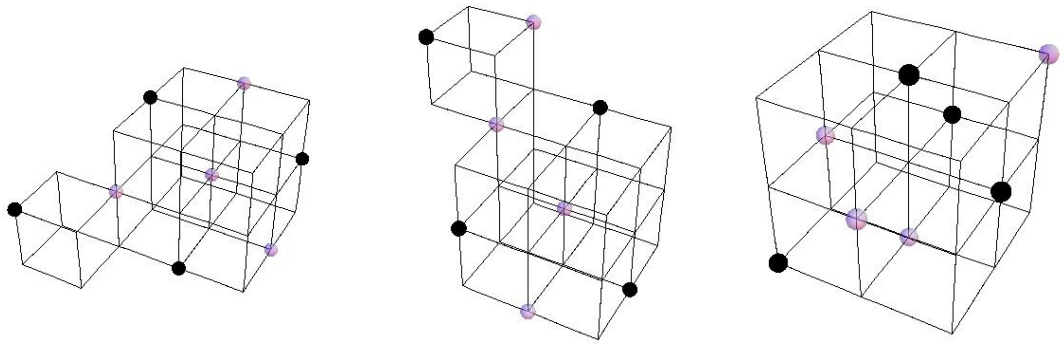

$Q1$ $Q2$ $Q3$

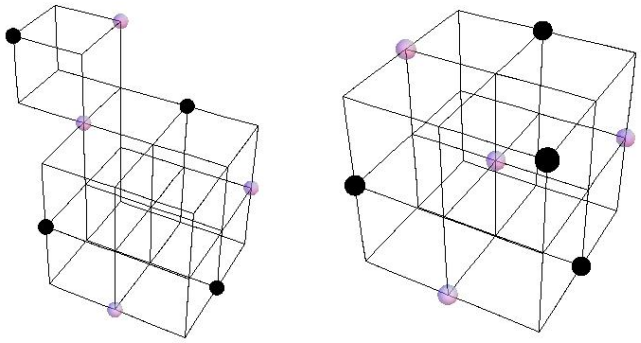

$Q4$ $Q5$

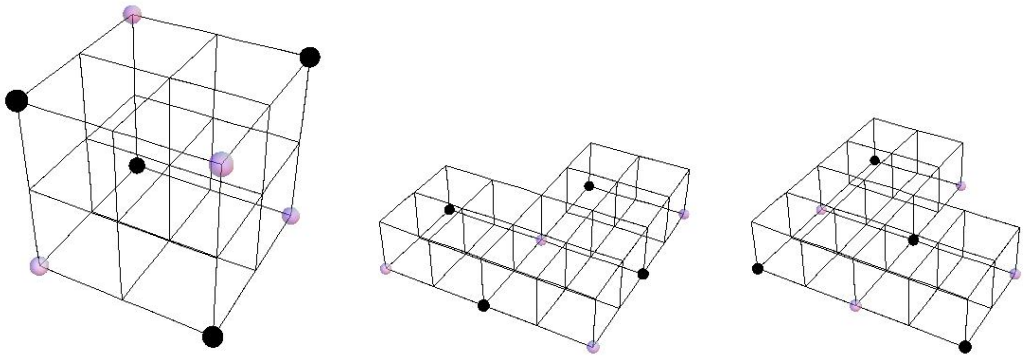

$Q7$ $Q8$ $Q9$

Figure 3.6: Selected configurations of tetramers.

Cluster energy	$U(c)$		ΔU	
System	NaCl:Pb	KCl:Pb	NaCl:Pb	KCl:Pb
$T1$	-18.52	-21.76	-0.1	-0.04
$T2$	-18.67	-21.88	-0.24	-0.16
$T3$	*-18.71	-22.14	-0.29	-0.42
$T4$	-18.52	-21.66	-0.09	0.06
$T5$	-18.43	*-22.34	-0.32	-0.49
$T6$	-18.29	-21.6	-0.18	0.25

Table 3.3: Cluster energies of trimers in eV. ΔU are energy differences between a cluster and its constituent dipoles (nn or nnn). Most stable configurations are marked *.

NaCl

The NaCl-Pb system exhibits very different pattern. Most stable dimer configuration, labeled $D4$, has lead atoms in 2nd next nearest neighbor sites and vacancies located between them. Comparison with $D1$ - corresponding to the same pattern where Pb atoms and vacancies exchanged positions indicates that it is more favorable if Pb ions are at greater distances and vacancies cluster between them. Addition of an impurity and a vacancy to this dimer leads to many configurations with small energy differences, but generally configurations with lower energy stay planar in {111} (e.g. $T2$ is more stable than $T4$) and have distances between Pb atoms greater than between vacancies. Emerging structure is a two-dimensional arrangement impurities and vacancies in {111}-Na-plane. The most stable trimer seems to be symmetrical hexagonal structure $T3$, though there is only small difference between the symmetrical $T3$ and crescent-shaped $T2$. Both in energy and structure, as the structures can be converted by one vacancy jump. Further addition of a dipole to this trimers leads to S shaped chain $Q2$ or to hexagon with dimer attached $Q4$, again with little energy difference and convertable by one vacancy jump.

For NaCl-$PbCl_2$ it is illustrative to project the {111} plane and schematize the growth processes there. The result is shown in Fig 3.7.

3.4 Larger clusters

The next step of the aggregation process is the growth of small clusters described in previous section to larger clusters. As explicit calculation of larger objects is more computationally expensive and also number of possible configurations grows very fast, we decided to change the means of modelling of large clusters. The general

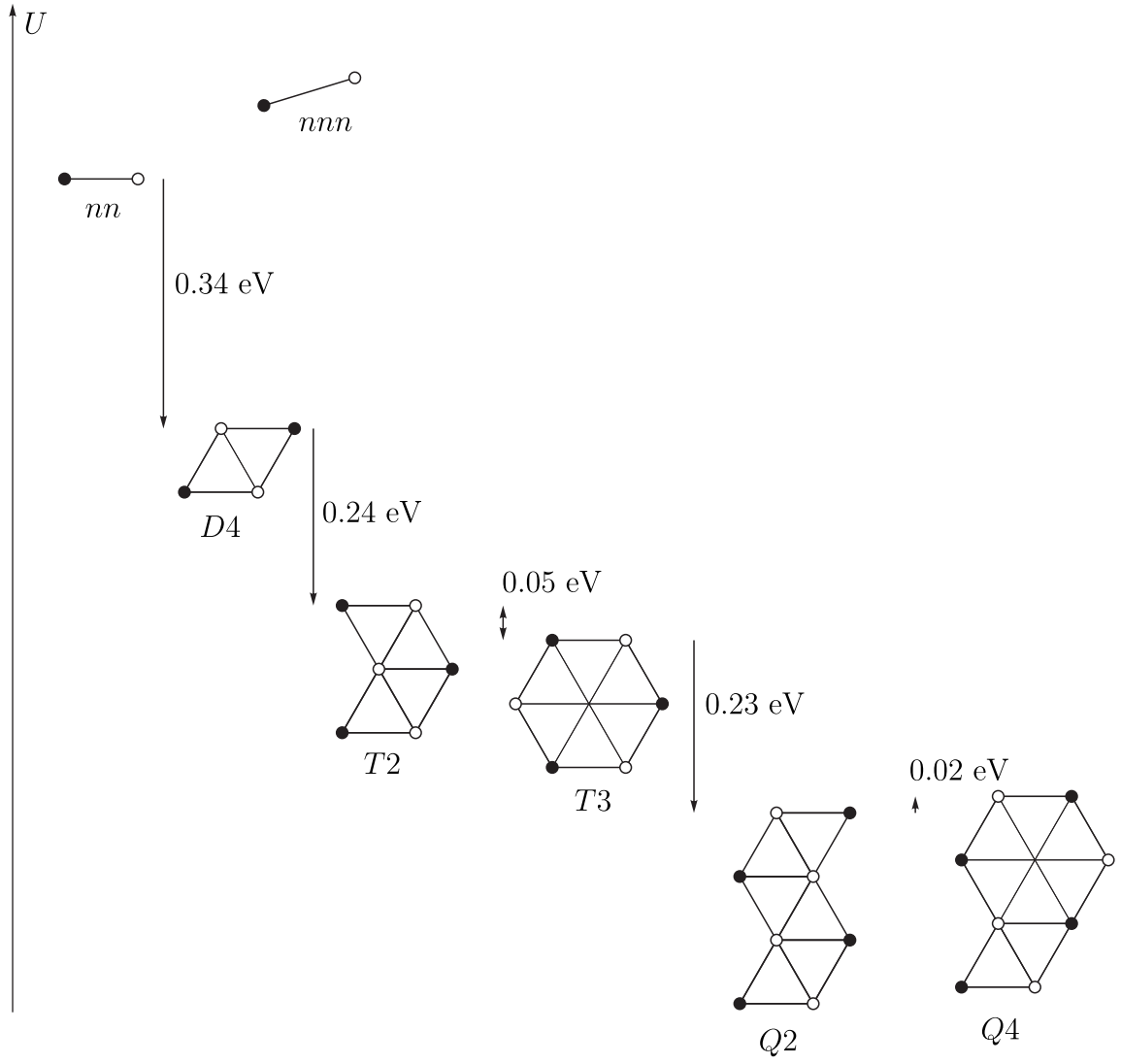

Figure 3.7: Energies of Pb-vacancy clusters in {111} Na plane of NaCl crystal. Realative positions of clusters represent energies of formation from their closest constituent parts.

Cluster energy	$U(c)$		ΔU	
System	NaCl:Pb	KCl:Pb	NaCl:Pb	KCl:Pb
Q1	-24.94	-28.98	-0.2	0.31
Q2	*-24.97	-29.22	-0.23	0.07
Q3	-24.89	-29.04	-0.15	0.26
Q4	*-24.95	-29.41	-0.21	-0.12
Q5	-20.70			
Q7	-24.72	*-29.77	-0.35	-0.34
Q8	-24.72	*-29.78	-0.36	-0.34
Q9	-24.73	-29.70	-0.36	-0.26

Table 3.4: Cluster energies of tertramers in eV. ΔU is energy difference between a cluster and its constituent dipoles (nn or nnn). Most stable configurations are marked *.

approach is to calculate "bulk" energy of the cluster and eventually also "interfacial" energy.

For computation of the energy of the "bulk" part we assume the structure is periodic.

Method of calculations

For the calculation of periodic structures energies we used classical lattice relaxation with supercell containing the layer and periodic boundary condition. Apart from that, interionic potentials and general computational framework was the same as in deffect calculations.

3.4.1 Single planar layer (NaCl)

In case of NaCl, small cluster results indicate that the clusters first grow in one plane. Hence, in this step, we calculate energies of various arrangements of Na, resp. Pb ions and vacancies in {111} Na-layer. A supercell was constructed from the planar arrangements in {111} plane and supplemented by several Cl and Na layers forming ordinary NaCl lattice, extending n layers in the direction perpendicular to the plane of the growing cluster structure (see Fig 3.8).

All arrangements with 2×2 and 3×2 2D-periodic structure unit cell were considered, along with some additional ones, inspired by energetically favorable cluster configurations, up to 4×4 2D unit cell.

Precisely speaking, the calculated system with this choice of supercell is an infinite ensamble of infinite planar layers of NaPb separated by n layers of NaCl. As coherency of the layer (resp. its interfaces) is imposed by the definition of the

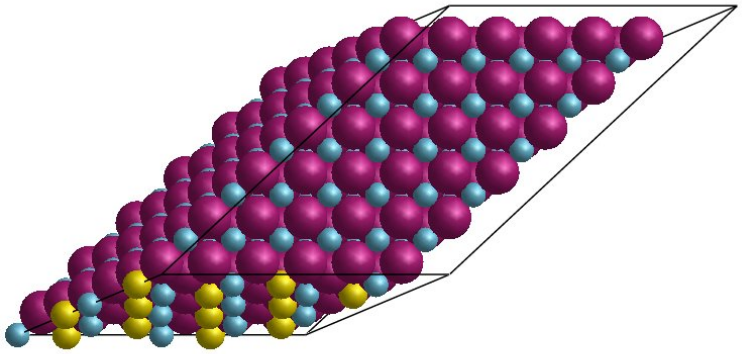

Figure 3.8: Example of supercell used for layer energy calculations. Pb atoms yellow, Na atoms blue.

supercell, interfacial energy and coherency strain created on the interface are mixed. We can partially overcome this problem by analysing cases with different number of attached NaCl layers. Case of individual layer is equivalent to $n \to \infty$, so it is in theory possible to split the interfacial and coherency strain by analysing the behaviour of the dependence of layer formation energy $\overline{U(L)}$ on n (defined later). In the numerical results, this dependence was observed, but was generally insignificant for relative comparison of different arrangements. It should be stressed, however, that energies of structures obtained in this way are not precisely comparable to defect energies calculated in previous section.

Examples of several such arrangements are given in Fig 3.9. Average energies of formation of arrangements layer per Pb atom were calculated. For layer L, supplemented by Cl layer and n NaCl layers the energy is

$$\Delta\overline{U(L)} = U(\text{cell}) - ((n+1)U(\text{NaCl}) + U(nn)), \tag{3.7}$$

if we consider formation of the layer from nn dipoles. The values of this energy are given in Table 3.5, along with ratio s of Na atoms in the layer replaced by Pb and vacancies ($s = 0$ for original layer consisting of Na atoms, $s = 1$ for layer consisting of only Pb atoms and vacancies).

The most stable arrangement found in this way is the one markedby $L7$, which can be thought of as a tiling of a plane with hexagonal pattern based on most stable trimer $T3$. It is possible in real crystal that the real arrangements will be different, or yet more complicated - limited class of arrangements was examined and effects like influence of dislocations were not considered. Nevertheless, even if this configuration minimizing energy is not the global minimum in whole energy landscape, some observations can be made: comparison of energy of formation per Pb atom $\overline{U(L)}$ of the $L7$ layer and respective quantity for small clusters $(U(c)/n - U(nn))$ shows the

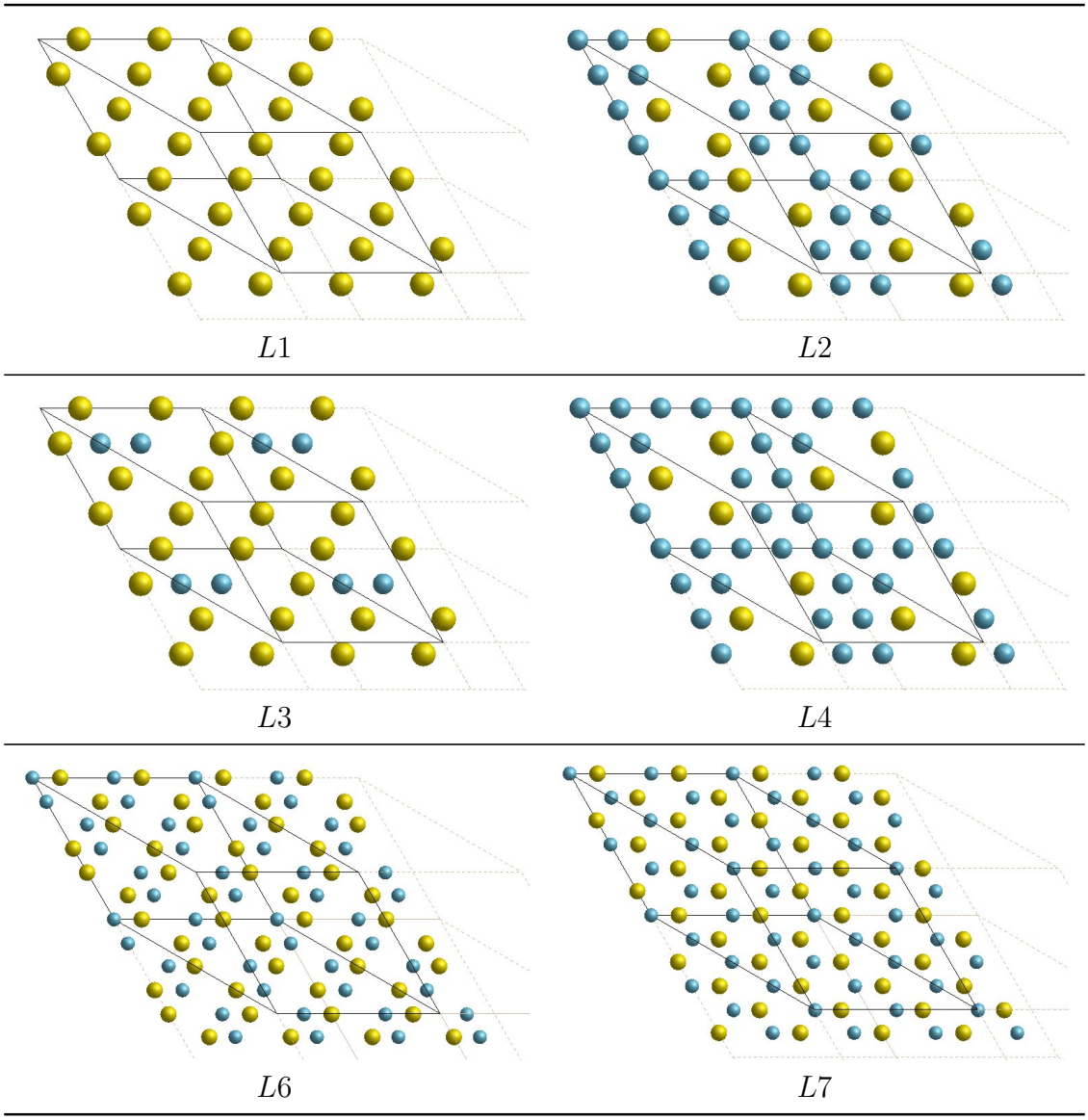

Figure 3.9: Examples of periodic arrangements in {111} plane. Na ions blue, Pb ions yellow.

Layer energy	s	$\overline{U(L)}$
$L1$	0.00	-0.31
$L2$	0.50	-0.23
$L3$	0.88	-0.16
$L4$	0.38	-0.24
$L6$	0.67	-0.14
$L7$	0.67	*-0.37

Table 3.5: Energies of stabilization of selected arrangements in eV, per Pb atom, relative to Pb in nn dipoles. Most stable configuration is marked *.

layer is more stable than small clusters, or in other words, energy is released by the growth from small to large clusters.

3.4.2 Multiple layers and transition to $PbCl_2$ in NaCl-matrix

Further growth can occur in direction perpendicular to the planar structure - which is a case analogous to surface growth. An attempt was made to explore this likely next stage and energies of various double- and triple-layer arrangements were calculated in a way similar to the single-layer case. Resulting energy differences between various structures based on $L7$ configuration were of order 0.01 eV per Pb atom; also energy difference between e.g. triple-layer $L7$ structure and triple-layer $L1$ structure shrank to 0.02 eV per Pb atom. So it is clearly beyond the precision of the presented calculations. Furthermore, for large clusters, probably the long-range coherency stresses (associated with the large planar coherent interface) will be relaxed by introduction of anticoherency dislocations, and the interface would loose coherency. Similarly, roughening of the surface will likely occur because of free energy contribution of configurational entropy.

It seems most probable that at some point, the existing aggregates undergo another transition - while staying in the shape of thin plates in {111} plane, the structure further deforms to full $PbCl_2$ structure and looses further coherency with the surrounding matrix. From comparison of $PbCl_2$ crystal in 001 plane (Fig 3.10) and NaCl crystal in {111} plane (Fig 3.11) it seems likely that the loss of coherency still will be only partial.

A scaling analysis of interfacial and strain energies suggests the decisive parameter for this transition is plate thickness. For thin plates consistitng of n metastable structure layers, interfacial energy is proportional to the area S of the platelet, while bulk lattice energy depends on volume $S.n$.

Stabilization energies given in Table 3.6 indicate the difference between intermittent planar phase and stable $PbCl_2$ is approximately -0.4 eV.

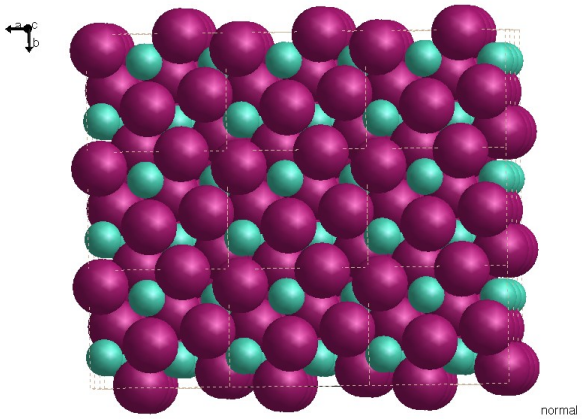

Figure 3.10: $PbCl_2$ crystal in 001 plane

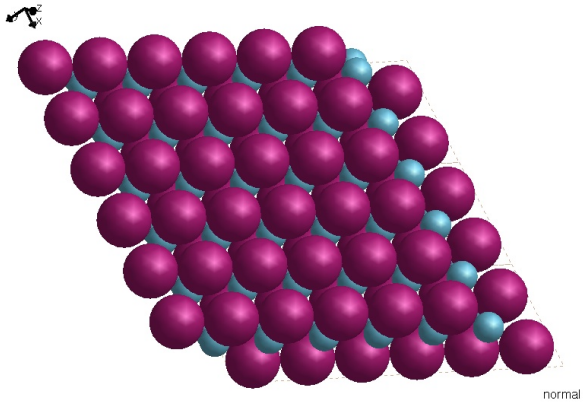

Figure 3.11: NaCl crystal in {111} plane, Cl ions violet

Structure	$\overline{U(L)}$
$D4$	-0.17
$L7$	-0.37
Suzuki phase	-0.34
$PbCl_2$	-0.74

Table 3.6: Energies of stabilization of selected arrangements in eV, per Pb atom, in NaCl.

Structure	$\overline{U(L)}$
$T5$	-0.30
Suzuki phase	-0.84
$PbCl_2$	-0.94

Table 3.7: Energies of stabilization of selected structures in eV, per Pb atom, in KCl.

3.4.3 Transition to $PbCl_2$ in KCl

As described previously, in KCl Suzuki phase most likely forms (Section 3.3.3).

As in previous section, we list energies of formation per Pb atom $\overline{U(L)}$ of various previously considered metastable objects and final $PbCl_2$ phase in Table 3.7. In this case, the difference between metastable Suzuki phase and stable $PbCl_2$, which is the driving force of further transformation, is only 0.1 eV.

Hence, further transition to full $PbCl_2$ structure is more difficult than in case of NaCl.

Chapter 4

Discussion

Conclusions from Chapter 3 can be compared both ith previous theoretical results, and also with experimental data. In summary, in lightly doped KCl-$PbCl_2$ system, Suzuki phase easily nucleates from the first aggregation steps, and further transition to $PbCl_2$ is hindered by high stability of this phase. This is in good agreement with experimental data. In comparison, NaCl-$PbCl_2$ systems exhibits complex behavior, where first metastable 2D phase completely coherent with host lattice nucleates and transition to $PbCl_2$ structure occurs after the plate-like particle reaches critical thickness. This result is different from some of the previous theoretical studies, but seems to be compatible with experimental measurements [36].

4.1 Comparison with previous results

4.1.1 KCl-$PbCl_2$

Results of presnted calculation agree with general understanding (e.g. [56]) that when ratio of dopant ionic radius to cation ionic radius is relivaly small, formation of Suzuki phase is likely. Bannon et al. [4] conclude that Suzuki phase is stable with respect to small clusters once formed. However, in these calculations, hexagonal cluster $T3$ appeared to be more stable than natural presursors to Suzuki phase (e.g. $T5$). Hence, initial steps of the process remained somewhat unexplained. As results of this work show natural pathway for Suzuki phase nucleation from direct precursors it seems likely this was caused by limited accuracy of calculations (this was noted in [4] as possible explanation).

4.1.2 NaCl-$PbCl_2$

Presented results for NaCl-$PbCl_2$ system are in agreement with Dryden's suggestion that first stage of nucleation takes place in $\{1, 1, 1\}$ plane via hexagonal structures. At variance with the original proposal, structures consisting of even number

of dipoles (dimers,tetramers,heptamers,...) are not significantly more stable than odd-numbered clusters (trimers, pentamers,...). Hence, nucleation proceeds by single particle processes, as is usual in many other systems.

Again, direct comparison is possible with results of Bannon et al. [4]. While trends of stabilization energies calculated here are the same, the dimer and tetramer Pb-vacancy clusters which are most stable ($D4, Q2$) are missing in Bannons study. Also, conclusion that trimer $T3$ is likely stable end point of aggregation sequence in these systems is different from our results.

Nature of expected planar metastable phase is very similar to plate zones described by Suzuki in NaCl-$CaCl_2$ system.

4.2 Experiment

Representative spectra of KCl-Pb and NaCl-Pb systems, as measured in FZU, are in Fig 4.1, resp. Fig 4.2.

While these spectral measurements seem to support conclusions for NaCl system, doubtless proof of nucleating phase structure would be possible only by X-ray methods.

4.3 Further prospects

In exploring multiple layer configurations and transition to $PbCl_2$ in NaCl (described in Section 3.4.2) some limitations of the present calculations were encountered. It would be very interesting to compute the energies of the supercells constructed there by more precise ab-initio methods (density functional calculation using full potential linearized augmented plane wave method seems most suitable). Also, such calculation with periodic boundary condition would allow detailed study of electronic structure and more direct correlation of optical measrements with calculation.

Also, it would be interesting to follow further development of morphology of large clusters, which could be best done using phase field methods.

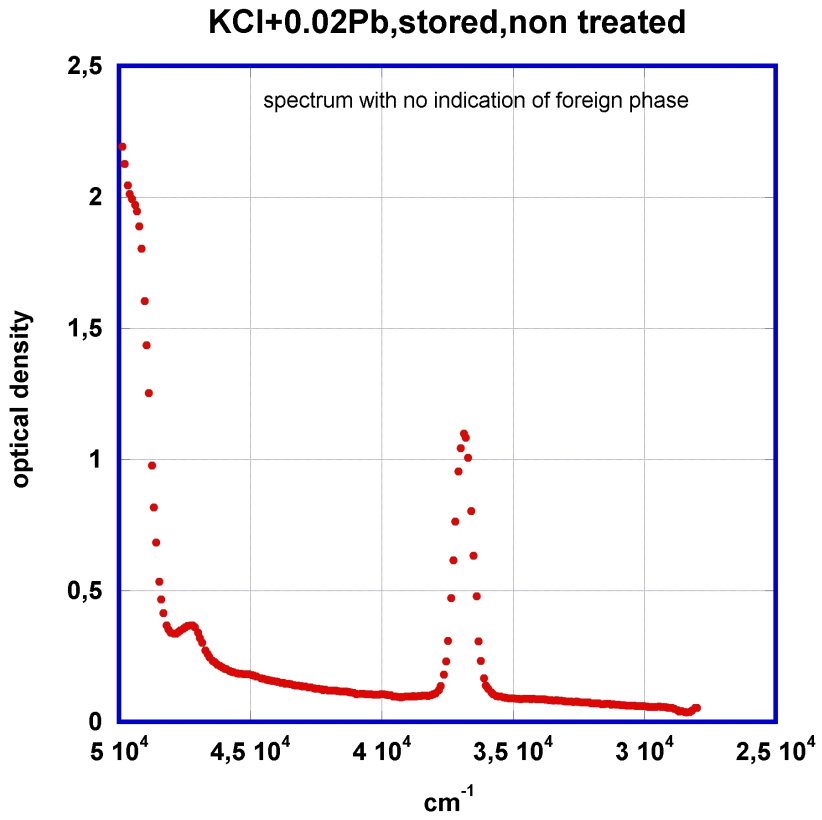

Figure 4.1: Absorption spectrum of KCl-Pb sample, annealed and kept at room temperature. [36]

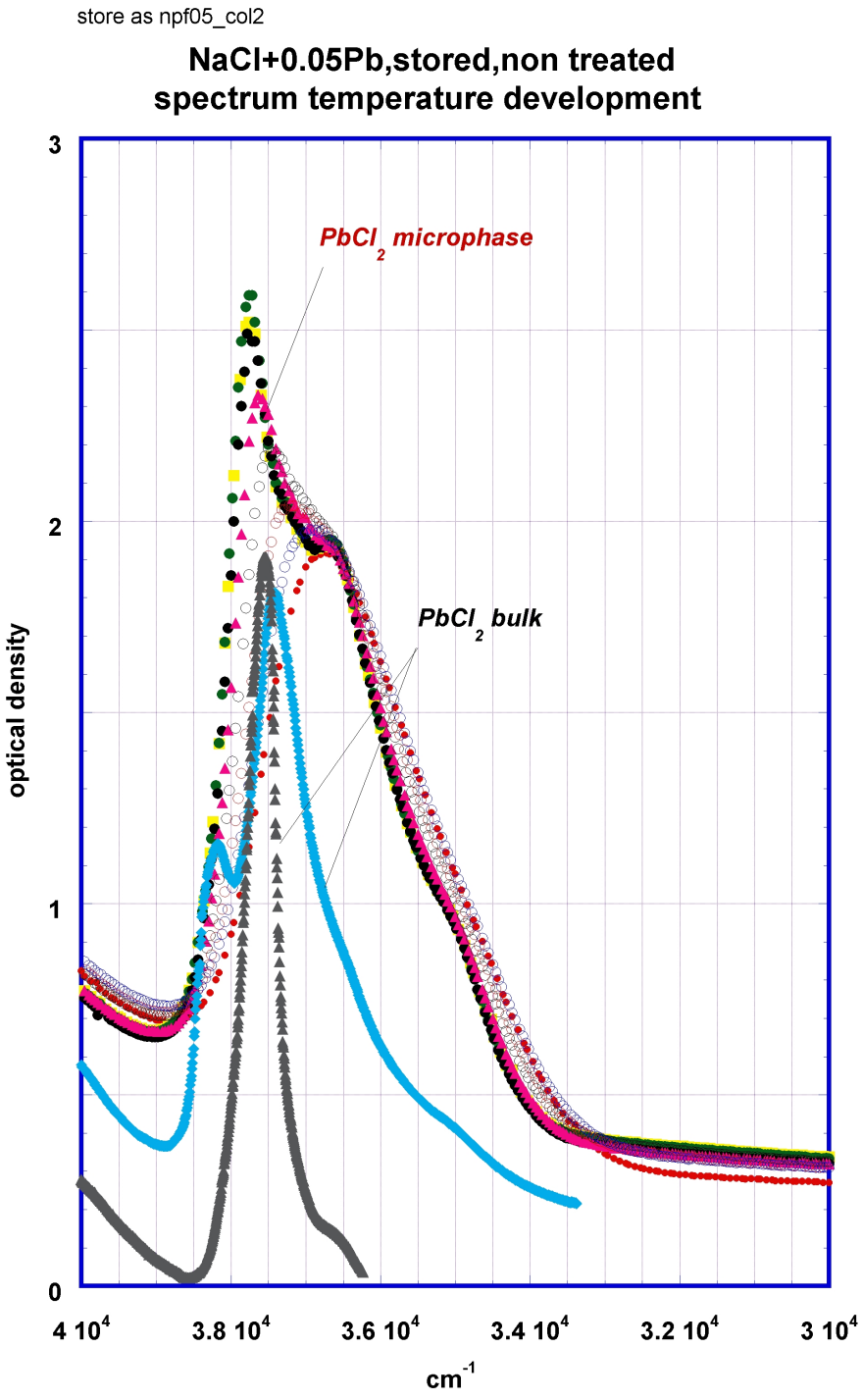

Figure 4.2: Absorption spectrum of NaCl-Pb sample. During nucleation spectrum exhibits complicated structure, probably related to complex nucleation process. [36]

Conclusion

In our work we analyzed early stage of nucleation in NaCl and KCl crystals doped with $PbCl_2$. In temperature region of interest to nucleation, Pb ions forms Pb^+ - vacancy complexes (dipoles).

First, defect energies of various configurations of small clusters of these dipoles (dimers, trimers, tetramers,...) were obtained by numerical lattice simulation based on interionic potentials. We have observed that in KCl system, the most stable cluster configuration (see Tables 3.3 and 3.4) have Suzuki phase structure. In contrast in NaCl most stable small clusters are planar arrangements of Pb ions and vacancies in $\{1, 1, 1\}$ Na plane. For schematic representation of first steps of the process see Fig 3.7.

In case of Pb-KCl, we have found natural nucleation pathway from single impurity-vacancy complex to Suzuki phase, which was not demonstrated in previous studies. Comparison of stabilization energies per Pb ion for ions embedded in small aggregates, bulk Suzuki phase and bulk $PbCl_2$ structure suggests formation of Suzuki phase hinders further transition to stable $PbCl_2$. Also, even small clusters have final Suzuki phase structure. This is in agreement with experimental measurements where no complex development of spectra during nucleation process is observed.

In case of Pb-NaCl, we have also found most probable nucleation pathway from single impurity-vacancy complex in nearest-neighbor position to stable dimer, trimer, tetramer, etc. In contrast to previous theoretical calculations [4], no stable "endpoint" of aggregation process was observed and our calculations suggests nucleation can easily proceed to large clusters. These most likely first stay planar, forming intermittent 2-D phase with specific structure fully coherent with surrounding NaCl lattice (see Fig. 3.9, configuration $L7$). Stabilization energies of embedding Pb atom in small clusters and planar phase indicate the growth process is energetically favorable. Further transition to stable $PbCl_2$ structure is most likely triggered by growing thickness of planar structure ("deposition" of several layers).

Our results do not confirm the previously described effect of stable nucleation endpoint. Nevertheless, they improve understanding of divalent impurity aggregation in alkali halides, particularly the formation of plate-zone structures in Pb-doped NaCl (similar to those observed by Suzuki [45][58] in Ca-NaCl system[1]).

[1]Not to be confused with Suzuki phase discovered also by Suzuki.

Appendix A

Computer simulations are important part of condensed phase physics, bridging the gap between fundamental physical theory and experimental results. Major progress has been achieved in this field both by development of new computational methods and increase in capabilities of available computer hardware.

A choice of a suitable computational method is very essential step in simulation of condensed phase system, and such choice is allways a tradeoff between precision, predictive power and computational cost.

We first very briefly describe some notable methodologies a their basic features; second, a choice of computational method for studied system is described; last, we describe chosen method and some parameters of the computations.

Computational methods can be roughly ordered by the level of simplification taken. On the most fundamental leve, the solid is described by Schrodinger equation, but exact solutions are not known for many-electron systems. Hence, approximate methods have to be used. Approxmations staying ont he quantum theory level are usually referred to as *ab initio* method - precisely a method which does not contain any empirical parameters beyond basic physical constants. Popular methos include Hartree-Fock method and related post-H-F methods, and density functional thoery-based methods. Generally density functional methods are computationally cheaper than post-H-F and are being used for larger systems, and all *ab initio*, are computainaly much more expensive than "atomistic" calculations

A.1 Atomistic methods

The level of description changes to "atoms", with semi-classical forces acting on them. Hybrid methods are recently developed.

A.1.1 Multi-body potentials

In reasonable simplification, we can express the energy by expansion in n-body interactions:

$$U = \frac{1}{2}\sum_{i,j} U_{ij} + \frac{1}{6}\sum_{i,j,k} U_{ijk} + \dots . \tag{A.1}$$

In many systems good approximation can be achieved by taking several first terms (e.g. for most organic systems four-body interactions are sufficient).

A.1.2 Pair potentials

In the simplest case, we can take only the first term and treat atoms simply as particles interacting with classical force (commonly given as potential). Forms of such potentials are often derived from quantum mechanical considerations, to account for

- Coulomb interaction (between ions)
- Dispersion
- exchange interaction (also known in this context as Pauli repulsion).

Well known example is Lennard-Jones potential taking the form

$$U_{ij}^{L-J} = \frac{a_{12}}{r_{ij}^{12}} - \frac{a_6}{r_{ij}^6} \tag{A.2}$$

with parameters a_{12} and a_6. The attractive r^{-6} term can be physically justified as the leading term in expansion of dispersion interactions. The repulsion term r^{-12} represents Pauli repulsion, albeit physically justified form would be exponential and choice of 12th power is more a matter of computational convenience, as it is square of the other term.

Other important example is the Buckingham[9] potential of the form

$$U_{ij}^{Buck.} = Ae^{\frac{r}{r_0}} - \frac{a_6}{r_{ij}^6} \tag{A.3}$$

with parameters A, r_0 and a_6. In this case the repulsion term takes more physical Born-Meyer form, but care must be taken to use the potential in realistic ranges of radii, as the energy has unphysical maximum at small separations and than diverges to $-\infty$ for $r \to 0$.

Pair potentials are sometimes generally referred to as "empirical potentials", but this is imprecise. We can arrive to truly empirical potentials if we get the parameters of potential of given form by fitting experimental data. On the hand, we can get these parameters also by fitting results of some calculation on more fundamental level (e.g. density functional theory). In such case the whole description could be independent of experimental data.

A.2 Computational cost

Generally computational cost of modelling n-atomic system decreases with level of simplification, or, in another view, simpler approaches allow simulation of larger systems. In present, post-Hartree-Fock methods and full-potential DFT are used for systems up to 10^2 atoms, simplified DFT up to 10^3 atoms, EAM for up to 10^5 atoms.

In principle aside is the question what we compute in the given approximation, for example, energy of a given structure, or most stable configuration of the system, dielectric or mechanical properties, or model some time evolution. When modelling motion of particles in the system, as in molecular dynamics (MD) approaches, numerical integration of the system is done, multiplying the computational cost.

A.3 Choice of method

Choice of suitable method in this study of nucleation of impurity dots in alkali halides depends on both physical and computational considerations.

First, alkali halides are very simple ionic materials, where lattice energy is dominated by Coulomb interaction (e.g. in NaCl), and the rest can be well described by simple interionic potential. While Coulomb potential has simple form, it is not easy to treat numerically, as in ionic solid the summation of contributions of individual ions is not absolutely convergent and special summation techniques have to be employed. Also, the force is relatively long-range and in case of defect, several adjacent layers of atoms act in relaxation. If we are concerned with precision of defect calculation, given limited computational resources, this leads to a tradeoff: more fundamental methods allow more precise evaluation of the energy close to the defect, but limit the number of atoms in "active cluster" for which full relaxation could be done. This could be overcome by hybrid methods, but at the cost of additional issue of correct join of regions treated by different methods.

Second, the desired results of the calculations are mainly defect energies. The largest defect clusters explicitly calculated have diameter about 6 times lattice constant. Hence, any model which may capture lattice relaxation even with minimal number of adjacent layers must contain at least hundreds of ions.

These considerations lead to choice of atomistic approach with pair interionic potentials for simulation of the system. This method was also successfully applied on the problem previously, and computer programs implementing the mothod are available. The calculations were done in GULP program, both theoretical and implementational description of the code is available in papers[31],[30]. Here we briefly describe the methods used for this work and detail used potentials and other parameters.

A.4 Lattice energy approach with interionic potentials

In chosen method, the solid is described as a set of ions where i-th ion with charge q_i has coordinates $\mathbf{r_n}$. The lattice energy is sum of pairwise energies:

$$U = \sum_{i,j \neq i} U_{ij}(r_{ij}, q_i, q_j). \tag{A.4}$$

Optimal structure can be found by minimizing energy as a function of $3n$ coordinates of studied $n-$atomic cluster or $n-$particle periodically repeating cell, which can be done by standard Newton-Raphson procedure.

A.4.1 Coulomb interaction

As mentioned before, Coulomb potential is simply

$$U_{ij}^{Coul.} = \frac{q_i q_j}{4\pi\epsilon_0 r_{ij}} \tag{A.5}$$

and summation (A.4) is not absolutely convergent in periodic systems; in spherical shells of growing radii r the number of ions rises as r^2, while the potential decreases only as r^{-1}. Convergence depends on suitable summation techniques, for example it is possible to choose charge neutral shells and sum over them. Another widely used technique for periodic systems is Ewald summation, in which the interaction split into short-range part, which converges rapidly in real space, and long-range part, which converges in reciprocal space.

A.4.2 Polarization effects

A successful and computationally cheap refinement of the point-charge model is inclusion of polarization effects. Widely used are the dipole model and shell model. In simulation of ionic solids the dipole model, while conceptually simpler, is computationally more demanding, so the shell model by Dick and Overhauser[21] was used in this study.

In this model, an atom is decomposed into "core" and "shell" parts with formal charges q_c resp. q_s, centered at $\mathbf{r_c}$ resp. $\mathbf{r_s}$, connected by a spring with stiffness k. (See Fig A.1). Formal charges of core and shell add up to formal charge of the ion $q_c + q_s = q_i$.

The formal charges and stiffness are basically convenient parameters chosen to fit experimental data or ab initio calculations on more fundamental level. Combination of the parameters with physical meaning is ionic polarizability in vacuum

$$U_{ij}^{Coul.} = \frac{q_i q_j}{4\pi\epsilon_0 r_{ij}} \tag{A.6}$$

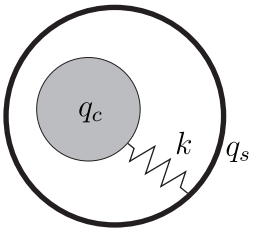

Figure A.1: Shell model

Coulomb interaction between different ions is taken to act between both cores and shells (that is core-core, shell-shell and core-shell). Short-range interactions act conventionally only on shells (shell-shell). Core and shell of one ion interact only by spring

$$U_{cs} = \frac{1}{2} k \left| \mathbf{r_c} - \mathbf{r_s} \right|^2 . \tag{A.7}$$

A.4.3 Interionic potentials

Various interionic potentials have been developed for alkali halides. for this study, we choose Set II. potentials by Catlow et. al.[13]. These potentials are based on fitting empirical data for 16 different alkali halides, and were previously successfully used in study of aggregation of divalent impurities.

The potentials in 2-nd neighbor interactions are of the so called "4-range Buckingham" form (See Fig A.2):

$$\begin{aligned} U(r) = A \exp\left(-\frac{r}{r_i}\right) \quad &\forall \quad r < r_1, \\ U(r) = a_0 + a_1 r + a_2 r^2 + a_3 r^3 + a_4 r^4 + a_5 r^5 \quad &\forall \quad r_1 < r < r_2, \\ U(r) = b_0 + b_1 r + b_2 r^2 + b_3 r^3 \quad &\forall \quad r_2 < r < r_3, \\ U(r) = -\frac{C}{r^6} \quad &\forall \quad r_3 < r, \end{aligned}$$

where coefficients in the second and third ranges are fixed by requiring continuity up to second derivative in junction points and fixing the minimum of the polynomials a r_2.

Parameters of the potentials for NaCl and KCl systems are given in Table A.1.

For nearest-neighbor interactions, simple repulsion potential is adequate:

$$U(r) = A \exp\left(-\frac{r}{r_i}\right) . \tag{A.8}$$

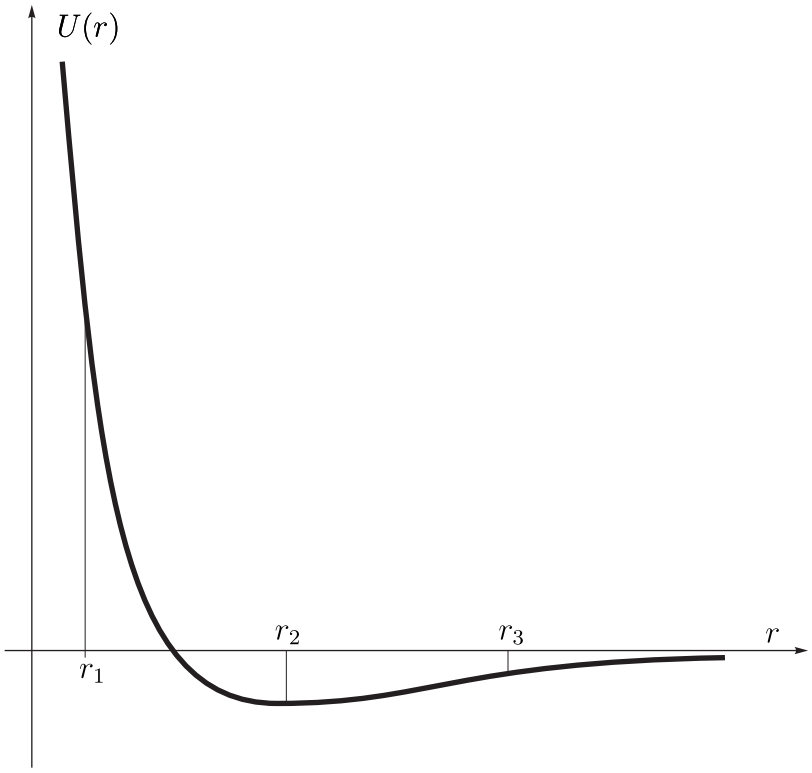

Figure A.2: Shematic plot of 4-range Buckingham potential

Ions	A (eV)	r_i (Å)	r_1	r_2 (Å)	r_3 (Å)	C (eV Å^6)
Cl-Cl	1227.2	0.3214	2.69	3.551	4.103	165.4
K-K	3796.9	0.2603	2.57	3.17	3.69	52.0

Table A.1: Parameters of 2-nd neighbor interaction from Set II. potentials[13]. To a good order Na-Na interactions can be neglected.

Ions	A (eV)	r_i (Å)
Na-Cl	872.7	0.3341
K-cl	4660.8	0.3007

Table A.2: Parameters of nearest neighbor interaction from Set II. potentials[13].

Ion	q_s (e)	k (eV.Å^{-2})
Na	2.128	96.44
K	-83.55	86032.0
Cl	-2.485	29.38

Table A.3: Parameters of shell model in Set II. potentials[13].

Ions	A (eV)	r_i (Å)
Pb-Cl	1620	0.340

Table A.4: Parameters of nearest neighbor interaction derived for Pb-Cl.

Parameters of the potentials are given in Table A.2.

Shell model parameters for the system are given in Table A.3.

A brief comparison with ab initio potentials derived from quantum mechanical calculations by Recio et. al. [52] was done for NaCl system and the results were qualitatively same (relative stabilities of various configuration do not depend on choice of potential, although absolute defect energies do).

No such tested potentials are available for Pb-ion interactions. Bannon et. al.[4] in study of the same system derived Pb potential from ab initio calculations based on Gordon and Kim electron gas model, while using the above described Set II. potentials for description of the host lattice. In our opinion this approach is problematic and better reliability can be achieved if the whole set of potentials is kept as coherent as possible. Hence, we decided to derive Pb-Cl interaction potential by fitting $PbCl_2$ structure data with simple potential (A.8) while taking Cl-Cl interaction from Set II. potentials. This leads to potential which describes Pb-Cl interactions in $PbCl_2$ with reasonable accuracy and at the same time is fully compatible with the rest of the potentials used in description of NaCl and KCl. Parameters of the potential are given in Table A.4. No attempt was made to describe polarizability of Pb ion, as [4] found the effects caused by inclusion of polarization are negligible.

A.4.4 Two-region strategy

In calculation of defects, two methods are widely used. In method of supercell, the defect is embedfed in large supercell and periodic structure based on this supercell is assumed. Physically, this resembles the case where average distance of defects is comparable to dimensions of supercell.]

Other possibility - chosen here - is the method known as “two region strategy” (or “Mott-Littleton procedure”, albeit contemporary implementations slightly differ

from the method used by Mott and Littleton). In current approach, the system is split into three parts - two spheres centered at "defect center" (usually mid-point of the ensamble of point defects) and rest of the lattice. In the inner sphere (Region I., active cluster, etc.) displacement of all ions is considered strong perturbation to the original lattice, and all the interactions are treated explicitly. In the outer sphere and the bulk (Region IIa. resp. IIb.), the perturbations are considered weak and can be approximated. Assuming it is sufficient to treat perturbations as harmonic, it is possible to eliminate self-energy of Region II. from the calculation and consider only energy arising from interaction with Region I. Furthermore, only a difference of energy between the defect configuration and configuration with ideal Region I. is important. This leads to a further approximation, where in Region IIa. only forces from defects are considered. In region IIb. which extends to infinity, it would be still difficult, so interaction with defects is replaced by interaction with multipole situated at defect center. Obviously, the quality of the approximation increases with increasing sizes of Region I. and Region IIb., and so does the computational cost.

In this work a variant of the two region strategy implemented in GULP[31, , p.68] was used for all defect calculations of Section 3.3. The size of regions I. and IIa. was fixed at 15 Åresp. 20 Å. Convergence was tested with sizes of Region IIa. up to 35 Å, and the difference in defect energies is smaller than 1%.

Bibliography

[1] International technology roadmap for semiconductors, 2009. *http* : *//www.itrs.net/Links/*2009*ITRS/Home*2009*.htm*.

[2] International technology roadmap for semiconductors - erm, 2009. *http* : *//www.itrs.net/Links/*2009*ITRS/*2009*Chapters*_2009*Tables/*2009_*ERM.pdf*.

[3] R.W. Balluffi, S.M. Allen, W.C. Carter, and R.A. Kemper. *Kinetics of materials*. 2005.

[4] NM Bannon, J. Corish, and PWM Jacobs. A theoretical study of vacancy-impurity association and of defect aggregation processes in divalently-doped silver halide crystals. *Philosophical Magazine A*, 52(1):61–72, 1985.

[5] S.D. Barrett and P. Kok. Efficient high-fidelity quantum computation using matter qubits and linear optics. *Physical Review A*, 71(6):60310, 2005.

[6] R. Becker and W. Döring. Kinetische behandlung der keimbildung in übersattigten Dämpfen. *Annalen der Physik*, 416:719–752, 1935.

[7] D. Bimberg, M. Grundmann, and N.N. Ledentsov. *Quantum dot heterostructures*. Wiley, 1999.

[8] A. Boca, A.D. Boozer, R. Miller, T. Northup, and H.J. Kimble. Reversible Transfer of Optical to Atomic States. In *APS Meeting Abstracts*, page 1274, 2007.

[9] RA Buckingham. The classical equation of state of gaseous helium, neon and argon. *Proceedings of the Royal Society of London. Series A, Mathematical and Physical Sciences*, 168(933):264–283, 1938.

[10] I. Buluta and F. Nori. Quantum Simulators. *Science*, 326(5949):108, 2009.

[11] E. Burstein, JJ Oberly, BW Henvis, and JW Davisson. A note on the distribution of impurities in alkali halides. *Physical Review*, 81(3):459–460, 1951.

[12] R. Capelletti and E. De Benedetti. Aggregation of divalent impurities in sodium chloride doped with cadmium. *Physical Review*, 165(3):981–985, 1968.

[13] CRA Catlow, KM Diller, and MJ Norgett. Interionic potentials for alkali halides. *Journal of Physics C: Solid State Physics*, 10:1395–1412, 1977.

[14] M. Chall, B. Winkler, P. Blaha, and K. Schwarz. Structure and properties of NaCl and the Suzuki phase Na6CdCl8. *J. Phys. Chem. B*, 104(6):1191–1197, 2000.

[15] JS Cook and JS Dryden. The Intensity of Dielectric Absorption in Alkali Halides as a Function of the Concentration of Divalent Cation Impurities. *Australian Journal of Physics*, 13:260, 1960.

[16] JS Cook and JS Dryden. An Investigation of the Aggregation of Divalent Cationic Impurities in Alkali Halides by Dielectric Absorption. *Proceedings of the Physical Society*, 80:479–488, 1962.

[17] J. Corish, JM Quigley, CRA Catlow, and PWM Jacobs. Dopant aggregation and precipitation in alkali halides doped with divalent ions. *Le Journal de Physique Colloques*, 41(C6):6–6, 1980.

[18] JH Crawford Jr. Aggregation of divalent metal impurity in alkali halide crystals. *Journal of Physics and Chemistry of Solids*, 31(2):399–409, 1970.

[19] M.D. Demetriou, N.M. Ghoniem, and A.S. Lavine. Effects of nucleation transience on crystallization kinetics under strongly nonequilibrium conditions. *The Journal of Chemical Physics*, 117:10739, 2002.

[20] P. Demo and Z. Kožíšek. Homogeneous nucleation process: Analytical approach. *Physical Review B*, 48(6):3620–3625, 1993.

[21] BG Dick and AW Overhauser. Theory of the dielectric constants of alkali halide crystals. *Physical Review*, 112(1):90–103, 1958.

[22] D.P. DiVincenzo. The Physical Implementation of Quantum Computation. *Fortschritte der Physik*, 48(9-11):771–783, 2000.

[23] JS Dryden and RG Heydon. Ultraviolet A-band absorption in NaCl: Pb2+ and clustering of lattice defects. *Journal of Physics C: Solid State Physics*, 16:5363, 1983.

[24] MI Dyakonov. Is fault-tolerant quantum computation really possible? *Future Trends in Microelectronics. Up the Nano Creek*, pages 4–18, 2007.

[25] JD Eshelby. The determination of the elastic field of an ellipsoidal inclusion, and related problems. *Proceedings of the Royal Society of London. Series A, Mathematical and Physical Sciences*, 241(1226):376–396, 1957.

[26] E. Farhi, J. Goldstone, S. Gutmann, and M. Sipser. Quantum computation by adiabatic evolution. *Arxiv preprint quant-ph/0001106*, 2000.

[27] L. Farkas. Keimbildungsgeschwindigkeit in übersattigten Dämpfen. *Z. physik. Chem*, 125:236–242, 1927.

[28] A.S. Foster, C. Barth, and C.R. Henry. Chemical Identification of Ions in Doped NaCl by Scanning Force Microscopy. *Physical review letters*, 102(25):256103, 2009.

[29] M.H. Freedman, A. Kitaev, M.J. Larsen, and Z. Wang. Topological quantum computation. *BULLETIN-AMERICAN MATHEMATICAL SOCIETY*, 40(1):31–38, 2003.

[30] J.D. Gale. GULP: A computer program for the symmetry-adapted simulation of solids. *Journal of the Chemical Society, Faraday Transactions*, 93(4):629–637, 1997.

[31] J.D. Gale and A.L. Rohl. The general utility lattice program (GULP). *Molecular Simulation*, 29(5):291–341, 2003.

[32] S.L. Girshick and C.P. Chiu. Kinetic nucleation theory: A new expression for the rate of homogeneous nucleation from an ideal supersaturated vapor. *The Journal of Chemical Physics*, 93:1273, 1990.

[33] L.K. Grover. A fast quantum mechanical algorithm for database search. In *Proceedings of the twenty-eighth annual ACM symposium on Theory of computing*, page 219. ACM, 1996.

[34] R. Hanson, LP Kouwenhoven, JR Petta, S. Tarucha, and LMK Vandersypen. Spins in few-electron quantum dots. *Reviews of modern physics*, 79(4):1217–1265, 2007.

[35] L. Jiang, JM Taylor, K. Nemoto, WJ Munro, R. Van Meter, and MD Lukin. Quantum repeater with encoding. *Physical Review A*, 79(3):32325, 2009.

[36] Polak K. Kcl-pb and nacl-pb experimental spectra. personal communication.

[37] D. Kashchiev. Solution of the non-steady state problem in nucleation kinetics. *Surface Science*, 14(1):209–220, 1969.

[38] J.L. Katz and H. Wiedersich. Nucleation theory without Maxwell Demons. *Journal of Colloid and Interface Science*, 61(2):351–355, 1977.

[39] KF Kelton, AL Greer, and CV Thompson. Transient nucleation in condensed systems. *The Journal of Chemical Physics*, 79:6261, 1983.

[40] C. Kittel and P. McEuen. *Introduction to solid state physics*. Wiley New York, 1996.

[41] Z. Kožíšek, P. Demo, and AM Sveshnikov. Size distribution of nuclei in a closed system. *The Journal of Chemical Physics*, 125:114504, 2006.

[42] Z. Kožíšek, K. Sato, P. Demo, and A.M. Sveshnikov. Homogeneous nucleation of droplets from supersaturated vapor in a closed system. *The Journal of chemical physics*, 120:6660, 2004.

[43] JL Krause and WJ Fredericks. The simultaneous diffusion of Pb2+ and Cd2+ in purified NaCl single crystals*. *Journal of Physics and Chemistry of Solids*, 32(12):2673–2684, 1971.

[44] D. Loss and D.P. DiVincenzo. Quantum computation with quantum dots. *Physical Review A*, 57(1):120–126, 1998.

[45] S. Miyake and K. Suzuki. X-ray Studies on the Structures of Solid Solutions NaCl-CaCl2. *Journal of the Physical Society of Japan*, 9:702, 1954.

[46] DL Moehring, P. Maunz, S. Olmschenk, KC Younge, DN Matsukevich, L.M. Duan, and C. Monroe. Entanglement of single-atom quantum bits at a distance. *Nature*, 449(7158):68–71, 2007.

[47] FRN Nabarro. The strains produced by precipitation in alloys. *Proceedings of the Royal Society of London. Series A, Mathematical and Physical Sciences*, 175(963):519–538, 1940.

[48] P. Neumann, N. Mizuochi, F. Rempp, P. Hemmer, H. Watanabe, S. Yamasaki, V. Jacques, T. Gaebel, F. Jelezko, and J. Wrachtrup. Multipartite entanglement among single spins in diamond. *Science*, 320(5881):1326, 2008.

[49] M.A. Nielsen. Cluster-state quantum computation. *Reports on Mathematical Physics*, 57(1):147–161, 2006.

[50] M.A. Nielsen and I.L. Chuang. *Quantum computation and quantum information*. Cambridge Univ Pr, 2000.

[51] D.A. Porter and KE Easterling. *Phase transformations in metals and alloys*. CRC, 2000.

[52] JM Recio, E. Francisco, M. Florez, and A.M. Pendas. Ab initio pair potentials from quantum-mechanical atoms-in-crystals calculations. *Journal of Physics: Condensed Matter*, 5:4975–4988, 1993.

[53] J. Schmelzer. *Nucleation theory and applications*. Vch Verlagsgesellschaft Mbh, 2005.

[54] F. Seitz. Color Centers in Alkali Halide Crystals. II. *Reviews of modern physics*, 26(1):7–94, 1954.

[55] P.W. Shor. Polynomial-time algorithms for prime factorization and discrete logarithms on a quantum computer. *SIAM review*, 41(2):303–332, 1999.

[56] AI Sors and E. Lilley. Anion Displacements and the Lattice Energy of the 6 NaCl· MCl2 Family of Structures. *Physica Status Solidi Applied Research*, 27:469–475, 1975.

[57] JE Strutt and E. Lilley. Structural aspects of clustering reactions in alkali halides doped with divalent impurities. *Physica Status Solidi Applied Research*, 33:229–239, 1976.

[58] K. Suzuki. X-ray Studies on the Structures of Solid Solutions NaCl-CaCl2 II. *Journal of the Physical Society of Japan*, 10:794, 1955.

[59] K. Suzuki. X-ray Studies on Precipitation of Metastable Centers in Mixed Crystals NaCl-CdCl2. *Journal of the Physical Society op Japan*, 16(1), 1961.

[60] H. Trinkaus and MH Yoo. Nucleation under time-dependent supersaturation. *Philosophical Magazine A*, 55(3):269–289, 1987.

[61] D. Turnbull and JC Fisher. Rate of nucleation in condensed systems. *The Journal of Chemical Physics*, 17:71, 1949.

[62] Wikipedia. Nitrogen-vacancy center — Wikipedia, 2010. [Online; accessed 7.4.2010].

[63] Wikipedia. Qubit — Wikipedia, 2010. [Online; accessed 7.4.2010].